THE GEOLOGICAL SOCIETY OF AMERICA®

Forearc magmatic evolution during subduction initiation: Insights from an Early Cretaceous Tibetan ophiolite and comparison with the Izu-Bonin-Mariana forearc

Jin-Gen Dai[1,†], Cheng-Shan Wang[1,2], Robert J. Stern[3], Kai Yang[1], and Jie Shen[1]
[1]*School of Earth Science and Resources and Research Center for Tibetan Plateau Geology, China University of Geosciences, Beijing 100083, China*
[2]*State Key Laboratory of Biogeology and Environmental Geology, China University of Geosciences, Beijing 100083, China*
[3]*Geosciences Department, University of Texas at Dallas, Richardson, Texas 75080, USA*

ABSTRACT

Subduction initiation is a key process in the operation of plate tectonics. Our understanding of melting processes and magmatic evolution during subduction initiation has largely been developed from studies of the Izu-Bonin-Mariana forearc. Many suprasubduction zone ophiolites are analogous to the Izu-Bonin-Mariana forearc sequence. However, whether there are differences between Izu-Bonin-Mariana subduction initiation sequences and suprasubduction zone ophiolites remains unclear. Here, we report field geological, geochemical, and geochronological data from mafic and felsic rocks in the Xigaze ophiolite (southern Tibet) mantle and crustal section; the same types of published data from both this ophiolite and the Izu-Bonin-Mariana forearc are compiled for comparison. The ophiolite section is intruded by various late-stage dikes, including gabbroic pegmatite, diabase, basalt, and plagiogranite. The compositions of clinopyroxene and amphibole suggest that gabbroic pegmatite formed from hydrous high-SiO_2 depleted melts, while whole-rock compositions of basaltic and diabase dikes show negative Nb and Ta anomalies, suggesting flux melting of depleted mantle. Along with the mafic rocks, plagiogranite has a roughly constant content of La and Yb with increasing SiO_2 contents, implying hydrous melting of mafic amphibolite. Early-stage pillow basalts exhibit geochemical affinities with Izu-Bonin-Mariana forearc basalts, but they are slightly enriched. Synthesized with the regional geological setting and compared with Izu-Bonin-Mariana forearc magmatism, we propose that the transition from mid-ocean ridge basalt–like lavas to subduction-related mafic and felsic dikes records an Early Cretaceous subduction initiation event on the southern flank of the Lhasa terrane. However, the mantle sources and the magmatic evolution in the Xigaze ophiolite are more variable than those for the Izu-Bonin-Mariana forearc.

INTRODUCTION

Plate tectonics is a unique feature of Earth that distinguishes it from other silicate planets in the solar system (Stern et al., 2018). Subduction initiation is critical for the operation of plate tectonics. The detailed processes of subduction initiation remain enigmatic and controversial, although spontaneous and induced mechanisms have been proposed (Stern, 2004; Stern and Gerya, 2018). In the last decade, we have learned much about subduction initiation, largely as a result of systematic geochronological and geochemical studies of the Izu-Bonin-Mariana forearc (Fig. 1A). Spontaneous subduction initiation commenced at ca. 52.5 Ma along a transform fault boundary between the proto–Philippine plate and the Pacific plate (Fig. 1C; Reagan et al., 2019). This was triggered by juxtaposition of the more buoyant lithosphere of the proto–Philippine plate next to older, denser Pacific plate lithosphere (Fig. 1B; Ishizuka et al., 2011, 2018). In the early stage of subduction initiation, forearc basalt was generated by decompression melting of depleted asthenospheric mantle to form what is now the forearc (Reagan et al., 2010, 2013). The association of sheeted dikes with pillow basalt in the forearc crust indicates that forearc basalt formed during seafloor spreading of the overriding plate between 52.5 and 48 Ma (Fig. 1C; Ishizuka et al., 2011). Continued lithospheric subsidence and percolation of slab-derived fluids resulted in flux melting of more depleted harzburgitic mantle, which generated boninites at ca. 48–44 Ma. Seafloor spreading also affected the back-arc region to form the Amami Sankaku Basin at ca. 49–48 Ma (Figs. 1B and 1C; Arculus et al., 2015; Hickey-Vargas et al., 2018; Ishizuka et al., 2018). Finally, normal tholeiitic and calc-alkaline arc magmatism occurred at ca. 44 Ma (i.e., 7–8 m.y. after subduction initiation) after the locus of magmatism had migrated westward away from trench (Ishizuka et al., 2011). The duration of forearc magmatism was less than 10 m.y. (Fig. 1C; Ishizuka et al., 2011, 2018).

Along with the forearc volcanic sequences and sheeted dike complexes, the underlying gabbro and mantle peridotite have also been observed, and thus a complete forearc sequence is documented (Fig. 2A; Ishizuka et al., 2011). Izu-Bonin-Mariana forearc lithospheric structure, which was generated during subduction initiation and is preserved in the Izu-Bonin-Mariana forearc, is similar to that of many suprasubduction zone ophiolites (Figs. 2A and 2B; Ishizuka et al., 2014). It is clear that many suprasubduction zone ophiolites preserve subduction initiation archives through igneous crust, upper-mantle residue, metamorphic soles (Parlak, 2016; Parlak et al., 2019), and overlying pelagic sediment (Stern et al., 2012). Contrary to the situation for the Izu-Bonin-Mariana forearc, which is mostly deep underwater and difficult to study, suprasubduction zone ophiolites exposed on land are readily studied, although deformation related to emplacement on land is often a complicating factor (Fig. 2). Therefore, the question remains: Can these suprasubduction zone ophiolites serve as analogues to the Izu-Bonin-Mariana subduction initiation sequence? If so, what can these volcanic rocks and intrusions tell us about subduction initiation magmatic evolution? If not, what is the difference between the Izu-Bonin-Mariana

Jin-Gen Dai http://orcid.org/0000-0002-6230-6801
†djgtibet@163.com.

GSA Bulletin; March/April 2021; v. 133; no. 3/4; p. 753–776; https://doi.org/10.1130/B35644.1; 13 figures; 1 supplemental file.
published online 5 August 2020

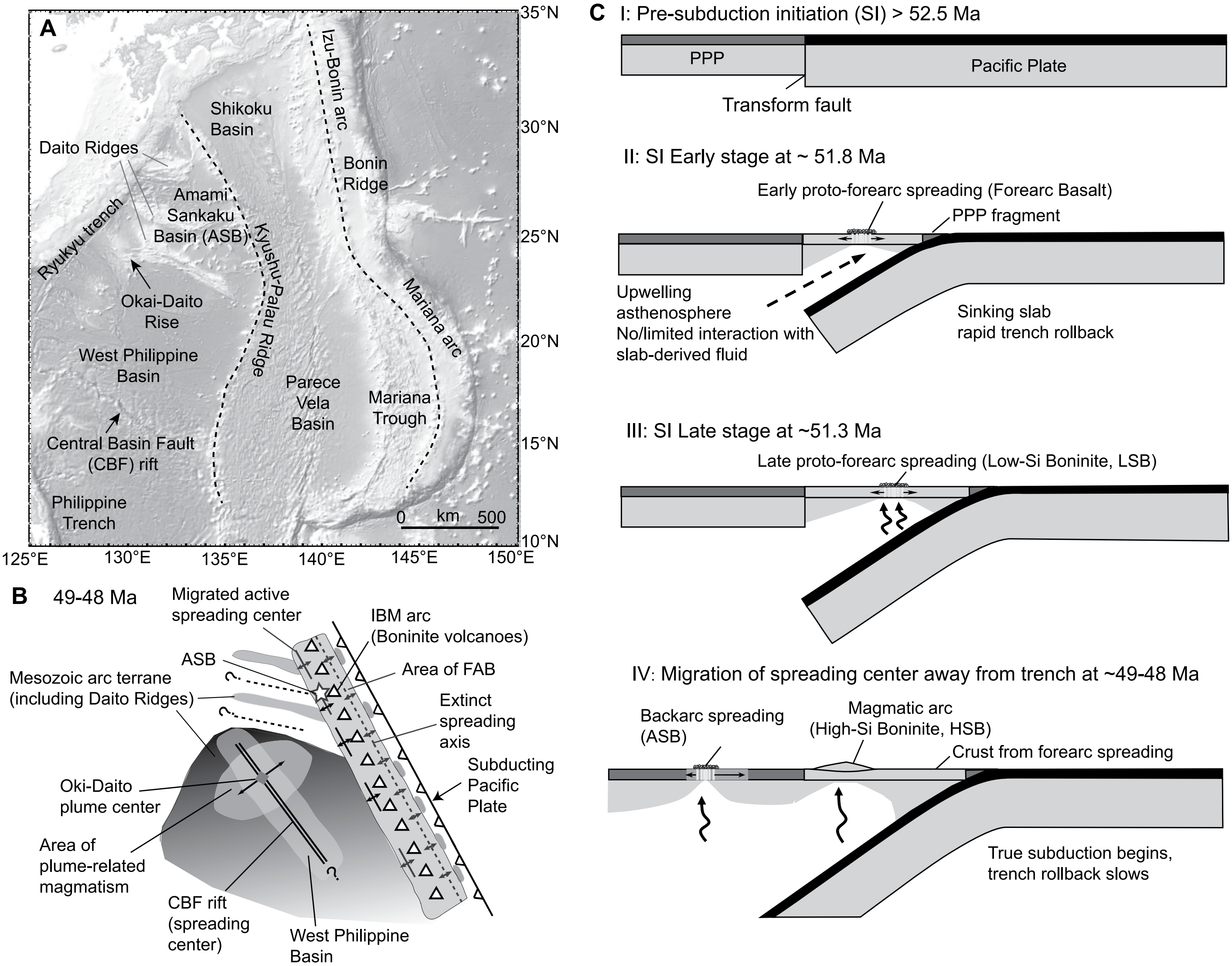

Figure 1. (A) Izu-Bonin-Mariana (IBM) arc trench system. (B) Schematic diagram showing tectonic reconstruction of the Izu-Bonin-Mariana arc and Philippine plate around 49–48 Ma (modified from Ishizuka et al., 2018). Seafloor spreading (including Amami-Sankaku Basin [ASB]) associated with subduction initiation formed ocean crust on overriding plate mainly composed of Mesozoic arc terrane. FAB—forearc basalt; CBF—Central Basin Fault. (C) Geodynamic evolution of Izu-Bonin-Mariana crust during subduction initiation (modified from Reagan et al., 2019). I—Presubduction initiation, when proto–Philippine plate (PPP) was in contact with Pacific plate along a transform fault. II—Spontaneous subduction initiation started at ca. 52.5 Ma, triggered by juxtaposition of more buoyant lithosphere of proto–Philippine plate next to older, denser Pacific plate lithosphere. Asthenospheric upwelling and decompression melting during near-trench seafloor spreading generated forearc basalt (FAB). III—Continued lithospheric subsidence and seafloor spreading generated forearc basalt and then late proto-forearc spreading basalt (low-Si boninite [LSB]). Melting of depleted mantle to generate low-Si boninite was aided by slab-derived fluids. IV—Back-arc spreading began around 49–48 Ma to form Amami-Sankaku Basin following subduction initiation. Amami-Sankaku Basin formed from a migrating spreading center associated with subduction initiation.

subduction initiation sequences and those of suprasubduction zone ophiolites?

In the Izu-Bonin-Mariana forearc, several types of volcanic rocks generated during subduction initiation record mantle melting, melt generation and migration, and crust-mantle interaction processes. Additionally, for suprasubduction zone ophiolites, late-stage intrusive rocks are widely distributed in the mantle peridotite. Such mantle intrusions are useful for revealing complex magmatic processes associated with subduction initiation because the associated volcanic rocks may be removed by erosion (e.g., Python and Ceuleneer, 2003). Both mafic and felsic melt intrusions have been reported in ophiolitic peridotites (Borghini et al., 2016; Piccardo et al., 2014; Python and Ceuleneer, 2003). Previous studies have tended to focus on either the mafic (Kaczmarek et al., 2015; Dilek et al., 1999) or felsic dikes in the upper mantle (Rollinson, 2009). Mechanisms for melt generation and multiple compositions remain poorly understood, including (1) whether mafic and felsic melts are coeval features and (2) whether their generation is related to subduction initiation.

The Xigaze ophiolite, located in the central part of the Yarlung Zangbo suture zone (the

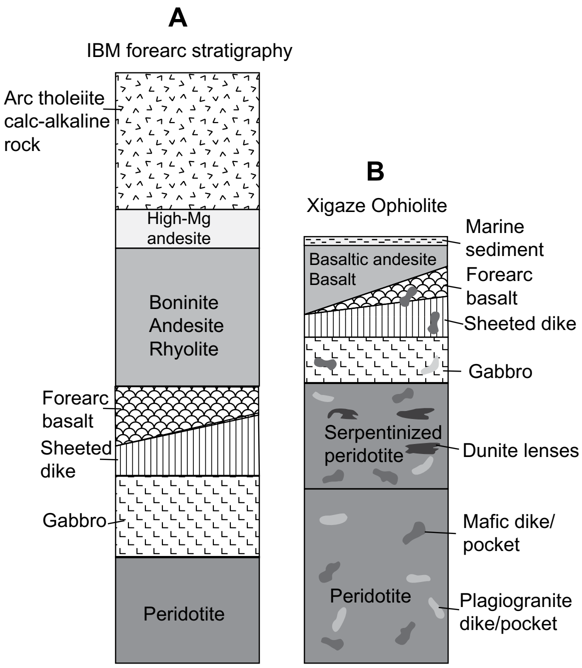

Figure 2. Schematic stratigraphic sections of (A) Izu-Bonin-Mariana (IBM) forearc (modified from Ishizuka et al., 2011) and (B) Xigaze ophiolite (modified from Girardeau et al., 1985a).

southernmost and youngest Tibetan ophiolite), is a remnant of Neo-Tethyan lithosphere (Hébert et al., 2012). It is well exposed in a region that is 5–20 km wide and ~100 km long. It has well-preserved mantle and crustal rocks but is dominated by mantle peridotite, which is mainly composed of variably serpentinized harzburgite associated with dunite and lherzolite (Girardeau et al., 1985a; Hébert et al., 2003; Nicolas et al., 1981). These mantle rocks are crosscut by abundant mafic dikes and sporadic plagiogranite dikes (Fig. 2B; Dai et al., 2013). Crustal rocks are dominated by basalt associated with sheeted diabase and limited cumulate gabbro (Fig. 3). Recent studies have increasingly revealed that the Xigaze ophiolite was generated in a forearc during subduction initiation (Figs. 4C–4E; Dai et al., 2013; Maffione et al., 2015; Xiong et al., 2016). Therefore, the Xigaze ophiolite mantle and crustal section offers unique opportunities to sample and investigate melt processes and magmatic evolution during subduction initiation.

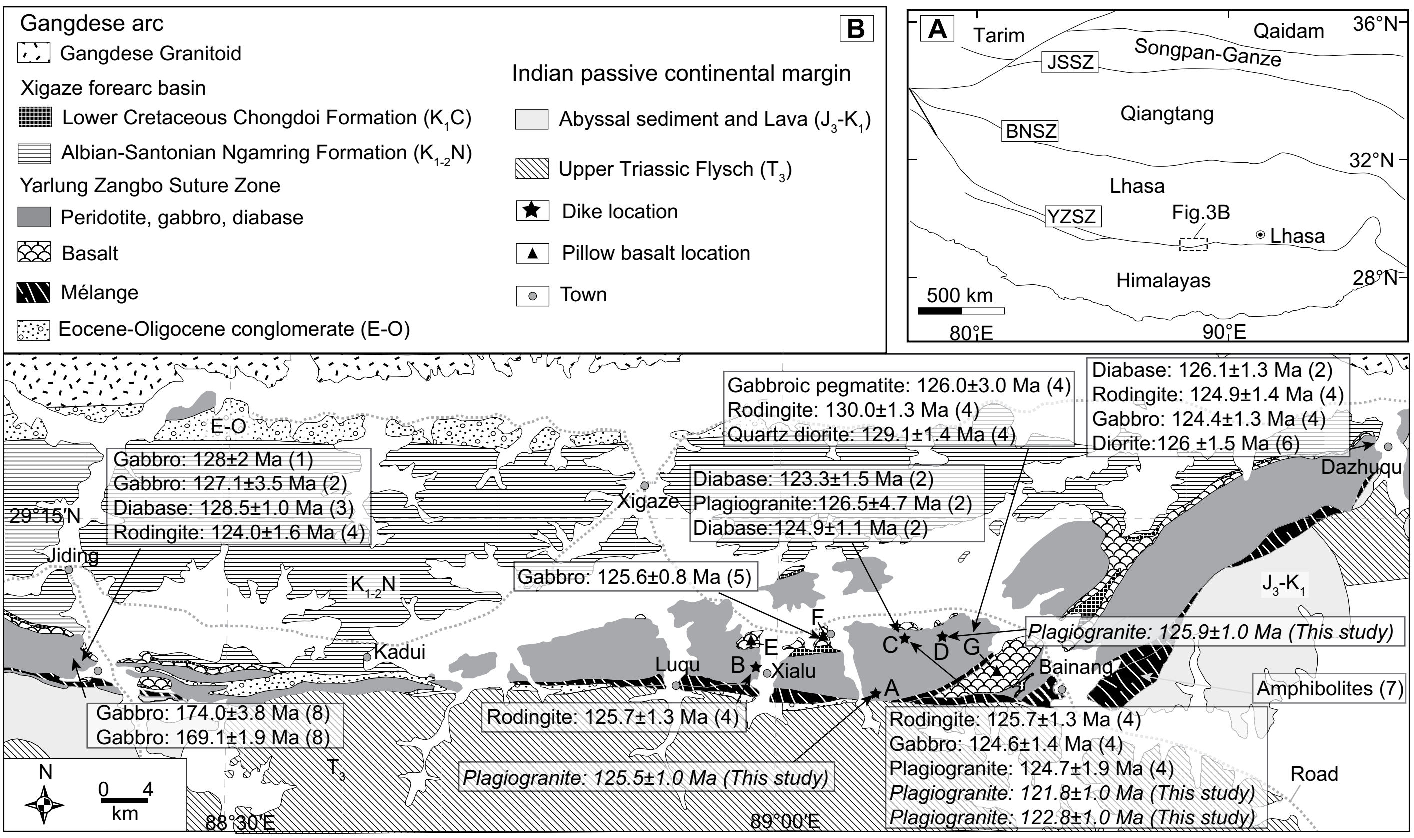

Figure 3. (A) Simplified tectonic map of the Tibetan Plateau showing major sutures (Yin and Harrison, 2000): JSSZ—Jinshajiang suture zone; BNSZ—Bangong–Nujiang suture zone; YZSZ—Yarlung Zangbo suture zone. (B) Geological map of the Xigaze area (Wang et al., 1987) showing the locations of dated samples (A–G). References: 1—Wang et al. (2006); 2—Dai et al. (2013); 3—Bao et al. (2013); 4—Zhang et al. (2016b); 5—Li et al. (2009); 6—Malpas et al. (2003); 7—Guilmette et al. (2009); 8—Wang et al. (2018).

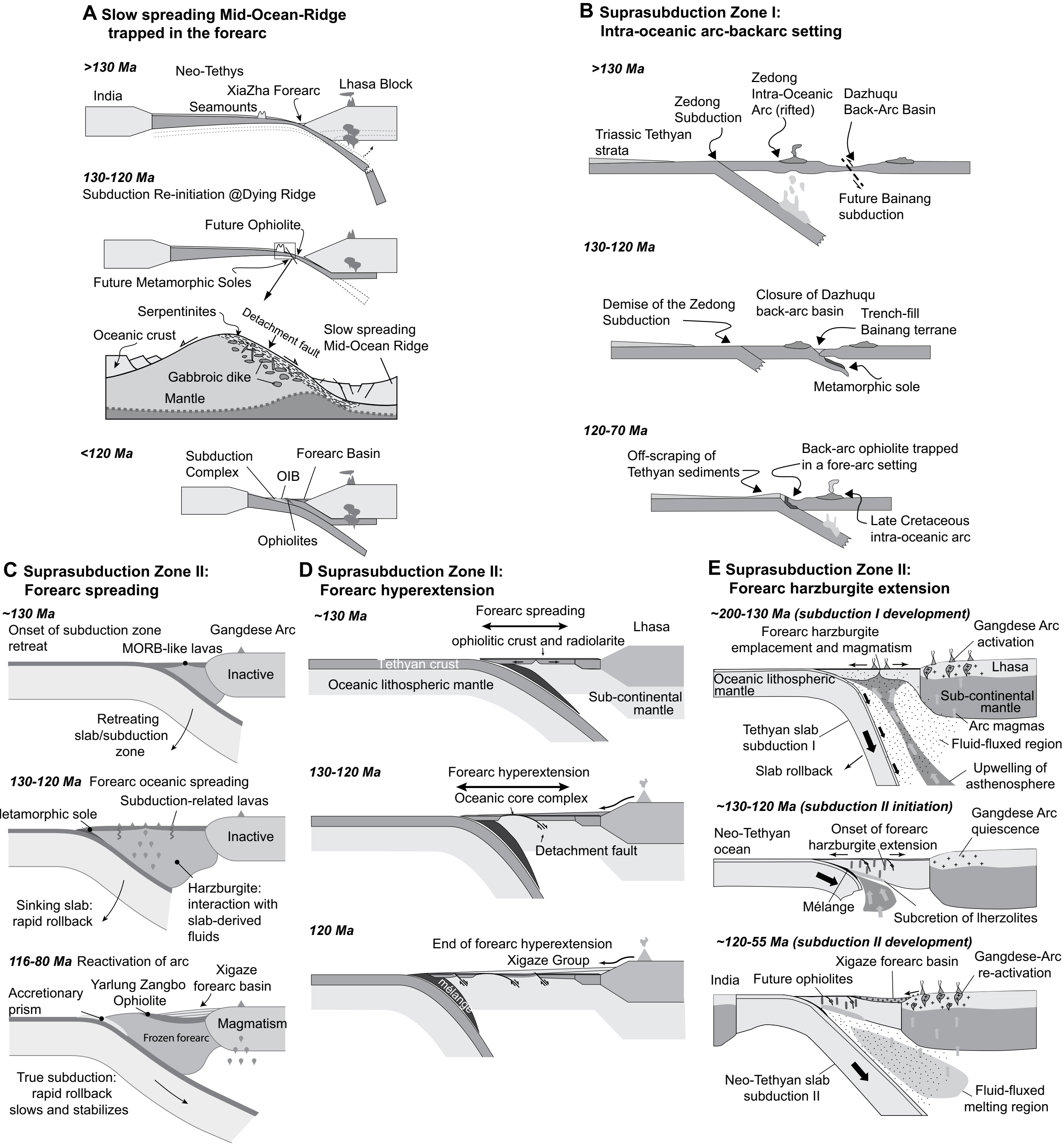

Figure 4. Proposed tectonic models for the Yarlung Zangbo ophiolite. (A) Slow spreading mid-ocean ridge trapped in forearc (Liu et al., 2014; Zhang et al., 2019). OIB—oceanic-island basalt. (B) Suprasubduction zone I: complex intra-oceanic arc–back-arc setting (Hébert et al., 2012; Guilmette et al., 2009). (C) Suprasubduction zone II: forearc spreading (Dai et al., 2013). (D) Forearc hyperextension (Maffione et al., 2015). MORB—mid-ocean-ridge basalt. (E) Forearc harzburgite extension and lherzolite subcretion (Xiong et al., 2016).

We conducted systematic field, petrological, mineral chemical (major and trace elements), Sr-Nd isotopic, and zircon U-Pb analyses on (1) various dikes, including gabbroic pegmatite, basaltic and diabase, and plagiogranite dikes, in both mantle and crustal sections; and (2) pillow basalt and sheeted diabase in crustal sections. Based on these data and our compilation of similar data for the Xigaze ophiolite and the

Izu-Bonin-Mariana forearc, the mechanisms for generating various mafic to felsic rocks in the mantle and basalts with sheeted diabase in the crustal section are discussed here. The different petrogenetic processes in conjunction with the magmatic evolution of the Gangdese arc and the depositional sequence in the Xigaze forearc basin strongly suggest that the Xigaze ophiolite formed during an Early Cretaceous episode of subduction initiation on the southern margin of the Lhasa terrane.

GEOLOGICAL AND TECTONIC SETTINGS OF THE YARLUNG ZANGBO OPHIOLITE

Geological Setting

The Yarlung Zangbo suture zone marks the southernmost and youngest suture in the Tibetan Plateau (Fig. 3A; Yin and Harrison, 2000). This suture includes remnants of the Neo-Tethyan oceanic lithosphere accreted to Eurasia (Allégre et al., 1984; Hébert et al., 2012). Four major lithotectonic units related to the Yarlung Zangbo suture zone occur in southern Tibet; from south to north, these are: (1) the accretionary prism, (2) the Yarlung Zangbo ophiolite, (3) the Xigaze forearc basin, and (4) the Gangdese arc (Dai et al., 2013). The Gangdese arc, located in the southern part of the Lhasa block, consists of latest Triassic to Eocene granitoids (Chu et al., 2011; Ji et al., 2009) and Cretaceous to Paleogene volcanic rocks of the Linzizong Group (Zhu et al., 2011). The Xigaze forearc basin, located south of the Gangdese arc, is an east-west belt that extends more than 500 km (Fig. 3B; Wang et al., 2012). Forearc basin strata are composed of the late Aptian to Coniacian flysch-dominated Xigaze Group (Chongdoi, Ngamring, and Padana Formations) and the Santonian to early Ypresian shallow-marine Cuojiangding Group (An et al., 2014; Dürr, 1996; Wang et al., 2012). The accretionary prism is composed of highly deformed serpentinized peridotite and a tectonic mélange of Triassic to Eocene sediment as a narrow elongate belt (Wang et al., 2012). The Yarlung Zangbo ophiolite comprises well-preserved to dismembered ophiolitic massifs. Previous studies documented that the Yarlung Zangbo ophiolite formed during 130–120 Ma (Dai et al., 2013; Li et al., 2009; Liu et al., 2016; Wang et al., 2006; Wu et al., 2014a; Zhang et al., 2016a; Zhang et al., 2016b). In the south, the Yarlung Zangbo ophiolite thrusts over a narrow belt of ophiolitic mélange that is composed of blocks of serpentinized peridotite, mafic rock, amphibolite, chert, limestone, and sandstone (Guilmette et al., 2009), while in the north, the Yarlung Zangbo ophiolite is overlain by flysch of the Xigaze Group (Dürr, 1996; Wang et al., 2012). The nonconformable depositional contact between Yarlung Zangbo ophiolite lava and sediment of the Chongdoi Formation defines the Yarlung Zangbo ophiolite as the base of the Xigaze forearc basin (An et al., 2014; Dai et al., 2015; Wang et al., 2017).

Tectonic Settings

Slow-Spreading Mid-Ocean-Ridge Model

Several tectonic models have been proposed for the Yarlung Zangbo ophiolite. In the early 1980s, detailed geological mapping was conducted on the Xigaze ophiolite in the central Yarlung Zangbo ophiolite, including the Dazhuqu massif to the Jiding massif (Fig. 3B). These studies revealed that the Yarlung Zangbo ophiolite did not form at a magma-rich mid-ocean spreading ridge, because of the paucity of mafic rocks, but it was instead generated at a slow-spreading ridge (Girardeau et al., 1985a; Nicolas et al., 1981). Limited thin crustal outcrops might be related to exhumation after ophiolite emplacement (Burg et al., 1987). This possibility was confirmed by thermochronological data from the Oligocene sediments within the Yarlung Zangbo suture zone, which reveal ~6 km (vertical) of rock removal (Carrapa et al., 2014).

The slow-spreading-ridge tectonic model was developed by Wu et al. (2014a) and his group (Fig. 4A). Zhang et al. (2016b) argued that Xigaze ophiolite basalts are typical normal mid-ocean-ridge basalts (N-MORBs) without influence from subduction-related fluids. However, the following lines of evidence argue against this conclusion: (1) Most mafic rocks show negative Nb anomalies and positive U and Pb anomalies, indicating that their source was affected by subduction-related fluids (Hébert et al., 2012); (2) although at least 85% of sedimentary Nd and Hf is recycled into the mantle, the Hf and Nd isotopic compositions of the Izu-Mariana arc lavas are not markedly different from those of MORBs (Chauvel et al., 2009). Therefore, the MORB-like Nd-Hf isotopic compositions do not rule out the possibility that mafic rocks were influenced by subduction-related fluids.

Liu et al. (2016) proposed that Xigaze ophiolite gabbroic rocks were generated beneath a fossil slow-spreading ridge because gabbro pods or dikes are associated with diabase dikes or sills, suggesting that the gabbros were exhumed when the diabase dikes were generated. Rapid exhumation of mantle peridotites and gabbroic rocks of the Xigaze ophiolite may have allowed intrusion of the diabase dikes and sills. The above arguments do not constrain the tectonic setting of the Xigaze ophiolite. If the Xigaze ophiolite had formed in a suprasubduction zone environment, the mantle peridotites and gabbroic rocks could also be intruded by diabase dikes. In addition, Liu et al. (2018) observed that gabbroic intrusions in the Jiding sequence are more evolved than Dazhuqu and Bainang gabbroic rocks, which are characterized by higher Cr_2O_3 but lower TiO_2 and rare earth element (REE) contents in both clinopyroxene and bulk compositions. They proposed that the lower oceanic crust within the Xigaze ophiolite is highly segmented and discontinuously distributed, similar to that exposed at modern slow- and ultraslow-spreading ridges. Such variations may be related to both magma evolution and magma source, since they also proposed that melt-crystal reactions played a key role in magma generation. More recently, Liu et al. (2019) proposed that Dazhuqu mantle peridotites experienced 0%–6% garnet-facies melting followed by 10%–18% melting in the spinel stability field, based on clinopyroxene trace-element modeling. This is similar to the degree of garnet-facies melting inferred for many mid-ocean ridge peridotites rather than forearc peridotites. The occurrence of abyssal peridotite is not strong evidence that the Xigaze ophiolite was generated in a slow-spreading mid-ocean ridge because a previous study revealed the occurrence of both fertile and depleted mantle in the Zedang area (Xiong et al., 2016). Specifically, previous studies have revealed that more than half of the Luqu peridotites (Fig. 3B) have ultrarefractory compositions indicated by both whole-rock and clinopyroxene compositions (Zhang et al., 2017).

The same group proposed a subduction re-initiation model at a dying mid-ocean ridge (Fig. 4A; Zhang et al., 2019), following previous studies by Guilmette et al. (2012). This interpretation was based on the high geothermal gradient recorded by the metamorphic sole in the Lhaze ophiolitic mélange, which has also been reported in other mélange massifs, including Bainang, Buma, and Saga (Guilmette et al., 2012). This model emphasized that the location of the subduction zone was close to the Eurasian continental margin (Zhang et al., 2019), while previous models proposed that subduction was intra-oceanic (Guilmette et al., 2012). This model proposed that (1) the entire Yarlung Zangbo ophiolite was a trapped remnant of MORB lithosphere that was generated in a slow-spreading mid-ocean ridge; and (2) the metamorphic sole originated from mid-ocean-ridge crust in the lower plate. However, the majority of the mid-ocean ridge was generally subducted, not accreted, just as illustrated by the currently subducting Nazca Ridge beneath the northern South American margin (Hampel et al., 2004). All these observations can be well explained in a subduction initiation model.

Suprasubduction Zone Model

Most studies of mineral and whole-rock geochemical data from the Yarlung Zangbo ophiolite reveal a heterogeneous mantle that possesses refractory whole-rock major-element compositions and U-shaped REE patterns (Dai et al., 2013; Zhang et al., 2017; Xiong et al., 2017). In addition, the high-Cr# spinels in most Yarlung Zangbo ophiolite peridotites (Hébert et al., 2003; Zhang et al., 2017; Xiong et al., 2017) indicate that they underwent hydrous melting. The mafic rocks show slight depletion in light REEs (LREEs) and have a small negative Ta-Nb anomaly, suggesting the influence of a subduction component. The abundances of incompatible elements in the mafic rocks are similar to back-arc basin basalts (Bédard et al., 2009; Hébert et al., 2012). Therefore, the Yarlung Zangbo ophiolite was proposed to belong to a complex intra-oceanic arc–back-arc setting, analogous to the Lau Basin (Fig. 4B; Aitchison et al., 2000; Hébert et al., 2003; Guilmette et al., 2009). However, there is no evidence for a slightly older intra-oceanic arc along the Yarlung Zangbo suture zone behind which a back-arc basin could form (Wu et al., 2014b). Instead, the associated Gangdese magmatic arc lies to the north, separated from the ophiolites by the Xigaze forearc basin (Fig. 3B).

Based on the geochemical similarities between basalts and late-stage mafic dikes in the Yarlung Zangbo ophiolite and forearc basalts and boninites in the Izu-Bonin-Mariana arc system, Dai et al. (2013) was first to propose that the Yarlung Zangbo ophiolite formed in a forearc spreading setting (Fig. 4C). This forearc spreading model was further developed in the following two models: (1) Forearc hyperextension: Paleomagnetic and geological field observations reveal the occurrence of extensional detachment faults in the Yarlung Zangbo ophiolite (Maffione et al., 2015). These exhumed mantle rocks and mélange on the seafloor were subsequently covered by forearc basin strata (Fig. 4D). Forearc hyperextension might help to explain the dismemberment of the Yarlung Zangbo ophiolite. (2) Forearc harzburgite extension and lherzolite subcretion: Both harzburgite and lherzolite outcrop in the Zedang ophiolite of the eastern Yarlung Zangbo ophiolite (Fig. 4E; Xiong et al., 2016). The equilibration temperature of lherzolite is 250–150 °C higher than that of the harzburgite, suggesting that harzburgites formed earlier (possibly at 200–130 Ma during an earlier episode of subduction) and at shallower levels than lherzolite. The authors proposed the coeval occurrence of the subcretion of lherzolites, intrusion of dolerite dikes, and doming and extension of overlying harzburgitic lithosphere during 130–120 Ma in the second stage of subduction (Fig. 4E).

FIELD OCCURRENCE AND PETROLOGY OF THE XIGAZE OPHIOLITE

The Xigaze ophiolite displays well-preserved sections from mantle to crustal rocks, together with overlying sedimentary strata (Fig. 2B). Marine sedimentary rocks consist of mudstone, chert, felsic tuffs, and fine-grained volcaniclastic deposits, and they are exposed along the northern margin of the Xigaze ophiolite, with late Barremian to late Aptian depositional ages (Figs. 2B and 3B; Ziabrev et al., 2003). The Xigaze ophiolite mafic sequence is thin (~2 km) (Girardeau et al., 1985b). A well-preserved sequence of pillowed lava occurs in several places, such as Qunrang, Deji, and Luqu. Minor cumulate gabbro has only been reported at the Dazhuqu, Bainang, and Jiding massifs (Liu et al., 2018). Sheeted diabase is rarely observed except at the Deji and Bainang massifs (Wang et al., 1987). The Xigaze ophiolite is dominated by mantle peridotites (Figs. 2B and 3B). These are variably serpentinized (Hébert et al., 2003) and are intruded by various dikes, such as diabase, rodingite, plagiogranite, and gabbroic pegmatite dikes (Fig. 2B).

Our field investigation and sample collection focused around seven massifs (locations A–D for gabbroic pegmatite, plagiogranite, diabase dike in the mantle and basaltic dike in the crust, and locations E–G for pillow basalt in Fig. 3B). Diabase dikes/pockets (for brevity, in some places, we use dikes for both) are widespread in the peridotite and are 0.3–4.5 m wide (Figs. 5A–5C). They are composed of plagioclase and clinopyroxene and sometimes are intensely altered (Fig. 6A). Gabbroic pegmatites occur as 3–4-m-wide pods or 0.1–0.3-m-wide dikes (Figs. 5D–5F). In some cases, peridotite enclaves occur within the gabbroic pegmatite dike (Fig. 5E). Gabbroic pegmatites are dominated by clinopyroxene megacrysts (Fig. 5F) with coarse-grained plagioclase (Figs. 6B–6D) and amphibole (Figs. 6D and 6E). The proportion of orthopyroxene is small in our samples. Accessory minerals are ilmenite, calcite, and prehnite (Figs. 6B and 6C). Clinopyroxene megacrysts range in length from 5 to 40 cm (Fig. 5F) and are generally euhedral (Fig. 6B). This mineral is commonly surrounded by amphibole, suggesting the formation of amphibole during late stages of fluid activity after crystallization of the clinopyroxene. Orthopyroxene is small in size, just 1–2 mm long (Fig. 6C), and is only found in location B in Figure 3B. Amphibole (1–2 mm in length; Fig. 6E) occurs as coronas around clinopyroxene. Plagioclase is subhedral (Fig. 6D), ranging in size 1–5 cm (Fig. 5D). Both clinopyroxene and amphibole are traversed by prehnite veins (Fig. 6B). Calcite veins are also observed in the gabbroic pegmatite.

Plagiogranite usually occurs as dikes from 0.3 m to 1 m wide (Fig. 5G; location D in Fig. 3B) or as pockets with an area of ~40 × 45 m (Figs. 5H and 5I; location C in Fig. 3B). At location A in Figure 3B, an association of gabbroic pegmatites and plagiogranite was observed, and their contact is diffuse (Fig. 5J). Some mafic rocks occur as enclaves in the plagiogranite (Figs. 5I and 5K). Most diabase enclaves present sharp contacts with the host plagiogranite (Fig. 5I). One sample (DJ12-20) was collected from these enclaves. The plagiogranite is medium grained and mainly consists of plagioclase and quartz, with minor amphibole, biotite, and orthopyroxene (Figs. 6F–6H), as well as common accessory minerals such as zircon and titanite. It is traversed by pumpellyite veins. Plagioclase is subhedral to euhedral and is partly altered into secondary minerals, mainly epidote and sericite. Amphibole is euhedral and ranges in color from brown to green (Fig. 6G). Orthopyroxene occurs both as megacrysts and as small grains (Fig. 6F). Quartz is commonly medium and fine grained, and anhedral to subhedral.

The intrusive section in the crust consisting of gabbro, diabase, and sheeted sill (Fig. 5M) is cut by basaltic and diabase dikes (Fig. 5L). Basaltic dikes are porphyritic with clinopyroxene and plagioclase phenocrysts (Fig. 6I). The volcanic section is mainly massive and pillow basalt (Figs. 5N and 5O). Secondary veins and amygdules of carbonate, quartz, and chlorite were observed in the pillow basalt.

GEOCHEMISTRY AND GEOCHRONOLOGY OF THE XIGAZE OPHIOLITE

New geochemical and geochronological high-quality data were obtained in this study. Detailed

Figure 5. Field photographs of the Xigaze ophiolite showing various mafic and felsic dikes in the mantle, and basaltic dike, sheeted sill, and pillow basalt in the crust: (A–C) diabase dike/pocket, (D–F) gabbroic pegmatite, (G–I, K) plagiogranite, (J) the association of gabbroic pegmatite and plagiogranite; (L) basaltic dike, (M) sheeted sill, and (N, O) pillow basalt. Cpx—clinopyroxene; Opx—orthopyroxene. Pencil for scale in A, person for scale in C, hammer for scale in H.

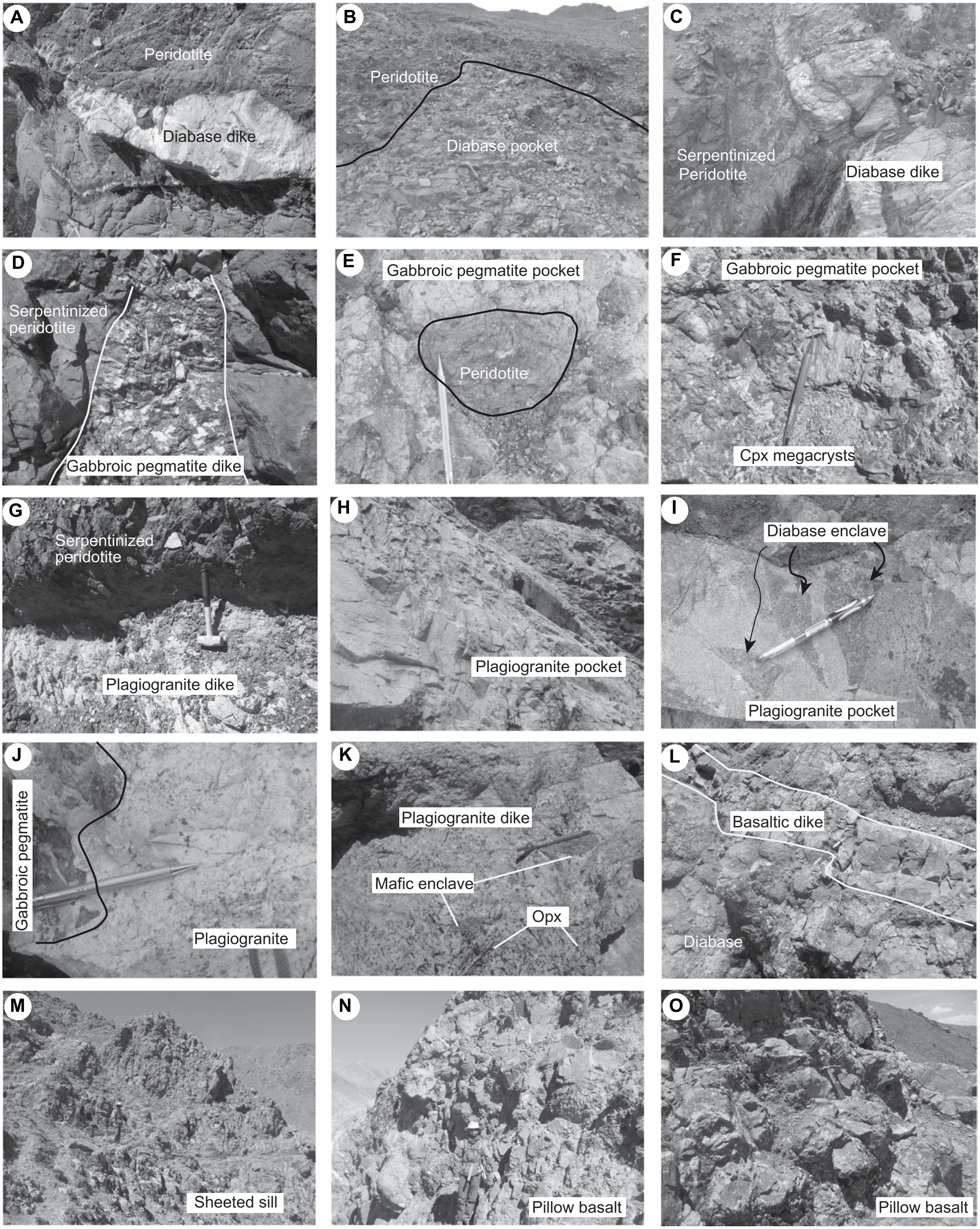
A
Peridotite
Diabase dike
B
Peridotite
Diabase pocket
C
Serpentinized Peridotite
Diabase dike
D
Serpentinized peridotite
Gabbroic pegmatite dike
E
Gabbroic pegmatite pocket
Peridotite
F
Gabbroic pegmatite pocket
Cpx megacrysts
G
Serpentinized peridotite
Plagiogranite dike
H
Plagiogranite pocket
I
Diabase enclave
Plagiogranite pocket
J
Gabbroic pegmatite
Plagiogranite
K
Plagiogranite dike
Mafic enclave
Opx
L
Basaltic dike
Diabase
M
Sheeted sill
N
Pillow basalt
O
Pillow basalt

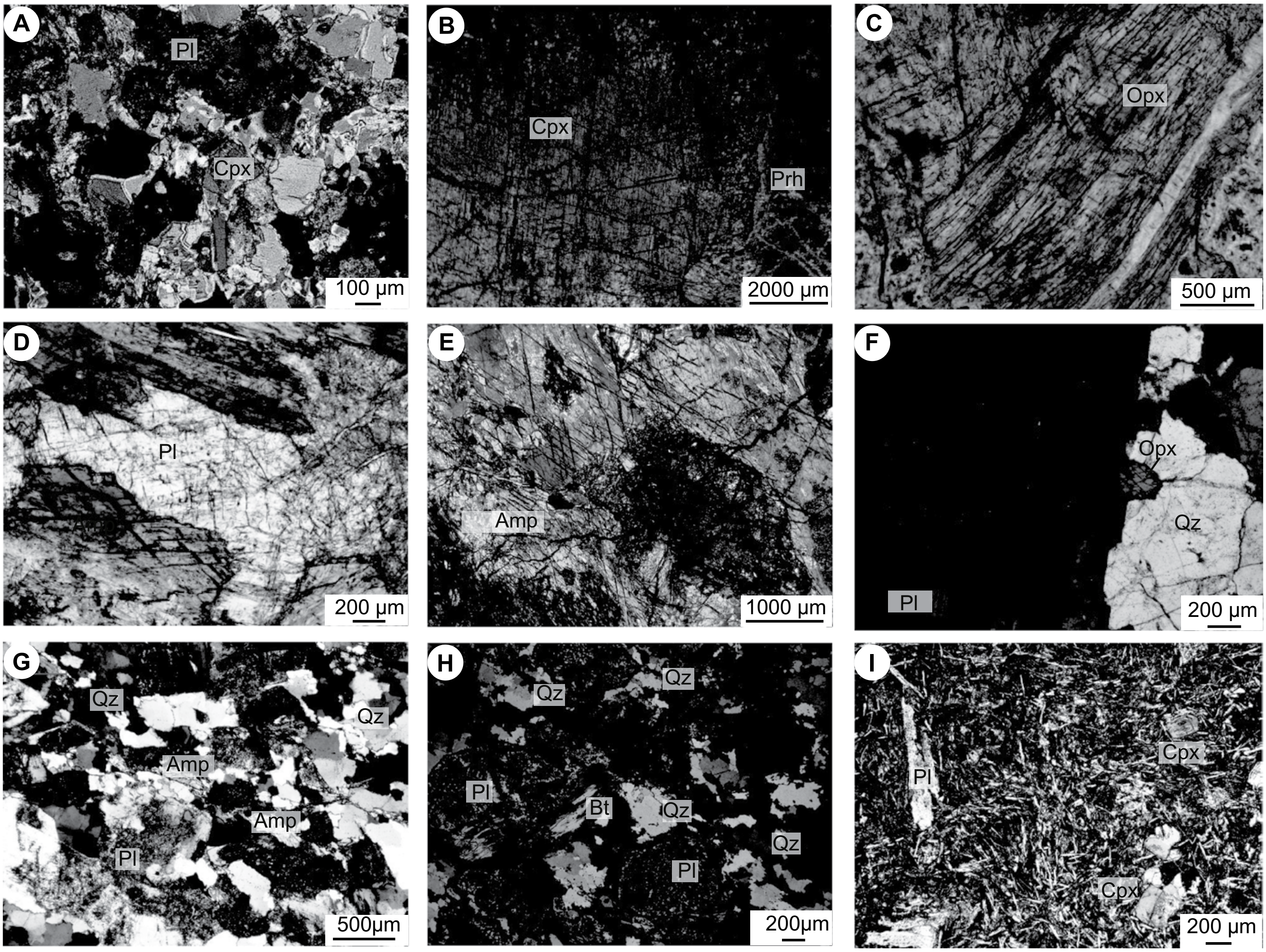

Figure 6. Photomicrographs of the Xigaze ophiolite: (A) diabase, (B–E) gabbroic pegmatite, (F–H) plagiogranite, and (I) basaltic dike. Pl—plagioclase; Cpx—clinopyroxene; Opx—orthopyroxene; Prh—prehnite; Amp—amphibole; Qz—quartz; Bt—biotite.

analytical methods are described in Text S1 in the Supplemental Material[1] (Andersen, 2002; Blichert-Toft and Albarède, 1997; J. Gao et al., 2002; S. Gao et al., 2003; Griffin et al., 2000; Jackson et al., 2004; Ludwig, 2008; Wu et al., 2006). In addition, previously published mineral and whole-rock geochemical and geochronological data from the Xigaze ophiolite were compiled (sources of data are listed in Text S1). Major- and trace-element compositions of clinopyroxene, orthopyroxene, and amphibole, whole-rock major and trace elements, Sr-Nd isotopic data, and zircon U-Pb and Lu-Hf data are given in Tables S1–S7, respectively (see footnote 1).

Mineral Chemistry and Thermometry

All clinopyroxenes in the gabbroic pegmatite plot in the diopside field (Fig. S1A; see footnote 1). They have Mg# [Mg/(Mg + Fe_{total})] ranging from 0.72 to 0.86. They contain 20.44–23.28 wt% CaO, 12.77–16.13 wt% MgO, 1.09–2.89 wt% Al_2O_3, and 0.2–0.44 wt% TiO_2. Their Cr_2O_3 contents span from undetectable to 0.2 wt% (Figs. S2A–S2C; Table S1). Clinopyroxenes display depleted LREEs (La_N 0.2–0.82) and flat middle (M)REE to heavy (H)REE (Gd_N/Lu_N 0.9–1.06, except for two samples with 0.58 and 0.71) patterns (where N represents chondrite-normalized and the values are from Sun and McDonough, 1989; Fig. 7A). In the primitive mantle–normalized incompatible element pattern, Ba and Sr are depleted compared with REEs; Nb, Ta, Zr, and Hf (high field strength elements [HFSEs]) show moderate to pronounced negative anomalies with respect to neighboring trace elements (Fig. 8A; McDonough and Sun, 1995). Two clinopyroxene megacrysts were separated and analyzed by X-ray fluorescence (XRF) for major elements and by ICP-MS for wet chemical analyses (bulk composition). Compared to the in situ analyses (microanalyses of clinopyroxene), the bulk compositions of the mineral separates showed higher Al_2O_3 contents and lower SiO_2 contents, but identical MgO and TiO_2 contents. The bulk analysis showed similar trace elements to those from microanalysis (Figs. 7A and 8A; Tables S1 and S4).

Orthopyroxenes from the gabbroic pegmatite have Mg# varying from 0.62 to 0.69, along with

[1]Supplemental Material. Detailed analytical methods in Text S1, major- and trace-element compositions of clinopyroxene, orthopyroxene, and amphibole, whole-rock major and trace elements, Sr-Nd isotopic data, and zircon U-Pb and Lu-Hf data in Tables S1–S7; Figures S1–S5. Please visit https://doi.org/10.1130/GSAB.S.12670091 to access the supplemental material, and contact editing@geosociety.org with any questions.

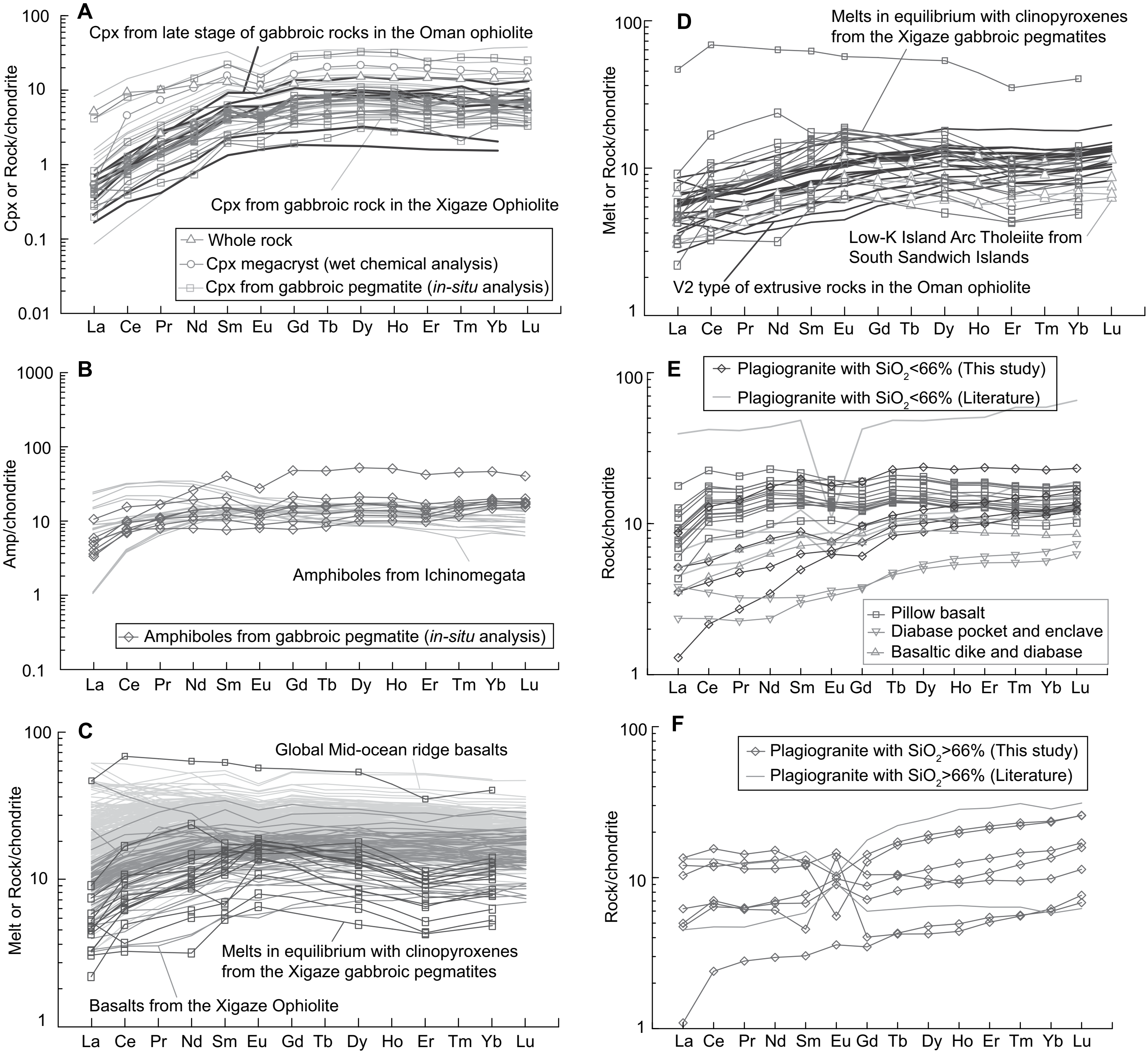

Figure 7. Chondrite-normalized rare earth element (REE) patterns of (A) clinopyroxenes (cpx), (B) amphiboles (B), (C, D) calculated melts in equilibrium with clinopyroxenes from gabbroic pegmatites, (E) pillow basalts, basaltic and diabase dikes, and (E, F) plagiogranites in the Xigaze ophiolite. The normalizing values are from Sun and McDonough (1989). Clinopyroxenes from the gabbroic dikes in the Oman ophiolite and the Xigaze ophiolite are from Yamasaki et al. (2006) and Koepke et al. (2009), and Liu et al. (2018), respectively. Amphiboles from Ichinomegata are from Coltorti et al. (2007). Compared data sources for plagiogranites are from Zhang et al. (2016b). The partition coefficients between clinopyroxene and silicate melt are from Gaetani et al. (2003). REE data for global MORBs are from GEOROC (http://georoc.mpch-mainz.gwdg.de/georoc); REE data for the low-K island-arc tholeiites are from Pearce et al. (1995); REE data for the V2 type of extrusive rocks in the Oman ophiolite are from Godard et al. (2003).

0.09–0.29 wt% TiO_2, 1.04–2.19 wt% Al_2O_3, 17.87–21.08 wt% FeO, 19.37–22.96 wt% MgO, and 1.08–1.88 wt% CaO, while orthopyroxenes from the plagiogranite have a limited range of Mg# from 0.64 to 0.65, along with 0.06–0.20 wt% TiO_2, 0.68–1.20 wt% Al_2O_3, 20.47–20.99 wt% FeO, 20.08–21.63 wt% MgO, and 1.01–1.93 wt% CaO (Table S2). All orthopyroxenes are enstatite (Fig. S1A). Only two grains from the gabbroic pegmatite were analyzed for trace elements, and they are excluded in the following discussion due to limited data.

All amphiboles are calcic. Amphiboles from the gabbroic pegmatite are magnesiohornblende, whereas those from the plagiogranite

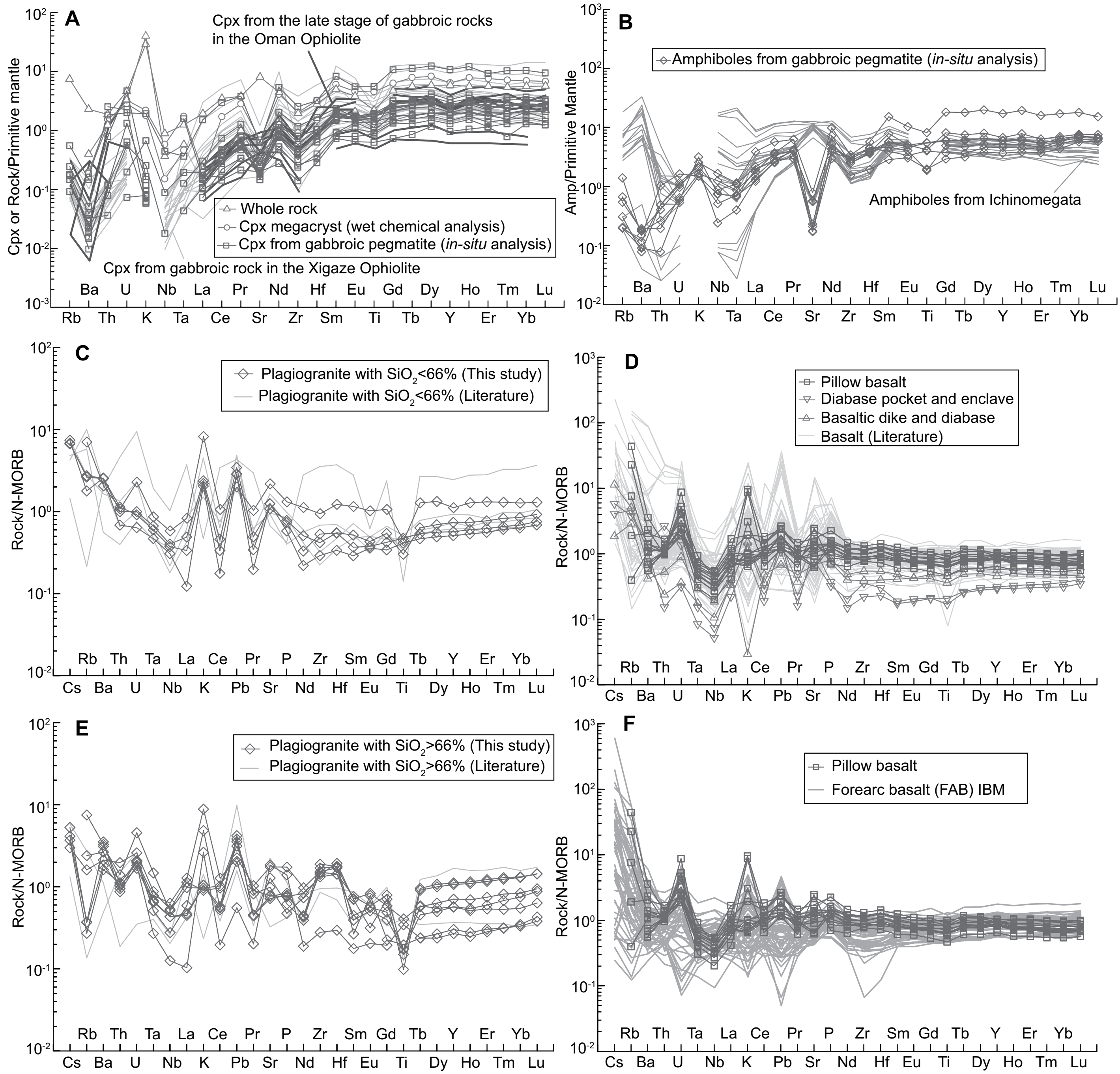

Figure 8. (A–B) Primitive-mantle–normalized trace-element patterns of (A) clinopyroxenes (cpx) and (B) amphiboles from gabbroic pegmatites in the Xigaze ophiolite; and (C–F) normal mid-ocean-ridge basalt (N-MORB)–normalized trace-element diagrams for plagiogranites (C, E), pillow basalts (D, F), and basaltic and diabase dikes (D). N-MORB normalizing values are from Sun and McDonough (1989). Data sources: mineral data are the same as Figure 7; plagiogranites are from Zhang et al. (2016b); basalts are from Bao et al. (2013), Chen and Xia (2008), Dubois-Côté et al. (2005), Malpas et al. (2003), Li et al. (2012), Niu et al. (2006), and Zhang et al. (2016b); forearc basalts are from Ishizuka et al. (2011, 2018) and Reagan et al. (2010, 2017). IBM—Izu-Bonin-Mariana.

vary from ferro-actinolite to ferro-hornblende (Fig. S1B; Leake et al., 1997). Amphiboles from the gabbroic pegmatite have Mg# values varying from 0.6 to 0.99. They have SiO_2 from 46.5 to 52.7 wt%, Al_2O_3 from 3.4 to 9.2 wt%, and MgO from 10.6 to 19 wt% (Figs. S2D–S2F; Table S3). Five analyses from the plagiogranite have Mg# values ranging from 0.36 to 0.39. The SiO_2, Al_2O_3, and MgO contents of these samples range from 47.5–50.7 wt%, 4.4–6.8 wt%, and 6.8–7.5 wt%, respectively (Table S3).

Amphiboles from the gabbroic pegmatite have nearly flat chondrite-normalized MREE-HREE patterns (Gd_N/Lu_N 0.75–1.19, except for two grains with 0.5 and 0.59) at 8–20 × CI (except for one grain at 27.5–52 × CI [Carbonaceous Ivuna chondrite]). Their REE contents are generally higher than those of clinopyroxene (Fig. 7B). They show LREE depletion (with La_N 3.2–5.9, except for one at 10.6) compared with MREE-HREE patterns. In the primitive mantle–normalized incompatible element patterns, Ba and Sr are depleted compared with neighboring trace elements; the HFSEs of Nb, Ta, Zr, Hf, and Ti show moderate to pronounced negative anomalies with respect to neighboring trace elements (Fig. 8B).

Geothermometers of clinopyroxene and amphibole were applied to the gabbroic pegmatites to constrain their thermal evolution. The clinopyroxene thermometer of Putirka (2008) yielded estimated temperatures between 1137 °C and 1191 °C (Table S1), with $K_D(\text{Fe-Mg})^{\text{cpx-liq}}$ ranging from 0.279 to 0.288, consistent with the referenced K_D values of 0.27 ± 0.03 (Putirka, 2008). The thermometer of Ridolfi et al. (2010) for amphibole yielded a range of 703–846 °C, which is considerably lower than values obtained from the pyroxene thermometry (Table S3).

Whole-Rock Major and Trace Elements

All lithologies are variously altered, and so major elements were normalized to 100% anhydrous for the following description and discussion. Two gabbroic pegmatites were analyzed, and the results show MgO contents of 8.7 and 10.3 wt%, and TiO_2 contents of 0.79 and 0.43 wt%. These rocks have SiO_2 contents of 51.8 and 52.1 wt%, Al_2O_3 contents of 15.7 and 13.6 wt%, and CaO contents from 10.1 to 12.2 wt%. Both samples plot within the basalt field (equivalent to gabbro based on whole-rock geochemical composition) in the total alkali-silica (TAS) diagram (not shown here). They show slightly depleted LREE and relatively flat MREE and HREE patterns. Both samples display modest Eu anomalies (Eu* = 0.79 and 1.38; Table S4). The positive Eu anomaly of one sample is similar to those of the gabbroic pegmatites reported in Zhang et al. (2016b). On the primitive mantle–normalized diagram, they generally are enriched in large ion lithophile elements (LILEs; e.g., K, Rb, U), and they show depletion in HFSEs (Fig. 8A).

The 11 plagiogranite samples exhibit a wide range of SiO_2 contents, ranging from 56.5 to 78.2 wt%, MgO from 0.3 to 3.4 wt%, Al_2O_3 from 12.2 to 18.7 wt%, Na_2O from 3.4 to 7.0 wt%, TiO_2 from 0.12 to 0.60 wt%, and K_2O from 0.12 to 1.15 wt%. They are characterized by low contents of K_2O and high Na_2O contents. MgO, Fe_2O_3(T), CaO, and TiO_2 decrease with increasing SiO_2, whereas other oxides such as Al_2O_3, Na_2O, K_2O, and P_2O_5 show little to no correlation (Fig. S3; see footnote 1). Plagiogranite samples do not lie on a continuous trend of the above major-element variations along with the gabbros, diabase, and basalts of the Xigaze ophiolite (Fig. S3). The plagiogranite samples are quartz normative and plot within the tonalite and trondhjemite field on the ternary anorthite-albite-orthoclase (An-Ab-Or) diagram (Fig. S5a; see footnote 1). Plagiogranite samples do not show any negative or positive relationship between SiO_2 versus trace-element plots (Fig. S4). Generally, most plagiogranite samples have similar trace-element concentrations with the mafic rocks of the Xigaze ophiolite. Their V contents are mostly lower than those of the mafic rocks, while their Zr concentrations are slightly higher than most mafic rocks (Fig. S4; see footnote 1), suggesting zircon accumulation in plagiogranites (Rollinson, 2009). Plagiogranite samples have low total REE contents (ranging from 8.7 to 38.5 ppm) and show LREE depleted patterns (La_N/Yb_N varying from 0.11 to 0.51) with slightly negative Eu anomalies in some samples (Figs. 7E and 7F). The LREE-depleted patterns are consistent with the original definition of plagiogranites (Coleman and Peterman, 1975), but they contrast with those of plagiogranites in mantle peridotite from other ophiolites, which are highly to slightly enriched in LREEs relative to HREEs (Rollinson, 2009, 2015). Plagiogranite samples are depleted in most HFSEs and enriched in LILEs with respect to normal mid-ocean-ridge basalt (N-MORB; Figs. 8C and 8E). They display significantly negative Nb-Ta-Ti anomalies, and they show enriched to depleted Zr and Hf contents relative to N-MORB.

The basaltic dike and its associated diabase have high MgO contents of 11.4 and 11.7 wt% with Mg values [Mg# = 100*Mg/(Mg + Fe^{2+})] of 72.8 and 76.6, and low TiO_2 contents of 0.58 and 0.46 wt% (Table S4). Both display LREE depletion (Fig. 7E), LILE enrichment, and significant depletion of HFSEs compared to N-MORB (Fig. 8D). One diabase enclave collected from the plagiogranite and one diabase pocket close to the plagiogranite pod have high MgO of 11.3 and 13 wt% with Mg values of 73 and 75.4, and the lowest TiO_2 contents of 0.26–0.22 wt%. These two samples also have the most depleted REE contents and show slightly LREE-enriched patterns (Fig. 7E). They also present more negative Nb and Ta anomalies than those of other mafic samples (Fig. 8D).

The pillow basalts are moderately to highly altered, as inferred from loss-on-ignition (LOI) values ranging from 2.0 to 7.6 wt%. They have MgO contents varying from 4.3 to 8.7 wt%, with Mg# values ranging from 50.3 to 72.4 (Table S4), SiO_2 ranging from 50.6 to 58.4 wt%, TiO_2 ranging from 0.6 to 1.3 wt%, and Al_2O_3 ranging from 14 to 17 wt%. They display relative flat to LREE-depleted patterns (Fig. 7E). In the N-MORB–normalized trace-element patterns, they show LILE enrichment and HFSE depletion (Fig. 8D).

Whole-Rock Sr-Nd Isotopes

Gabbroic pegmatites have initial $^{87}Sr/^{86}Sr$ ratios of 0.70346 and 0.70604 and initial $^{143}Nd/^{144}Nd$ ratios of 0.512944 and 0.513218, with $\varepsilon_{Nd}(t)$ values of +9.1 and +14.5 (Table S5). The clinopyroxenes have initial $^{87}Sr/^{86}Sr$ ratios of 0.70378 and initial $^{143}Nd/^{144}Nd$ ratios of 0.513178 and 0.512934, with $\varepsilon_{Nd}(t)$ values of +13.7 and +8.9. One gabbroic pegmatite and one clinopyroxene plot within the field of Xigaze ophiolite mafic rocks. Specifically, their isotopic values are also similar to those of gabbro samples from the Xigaze ophiolite but with low initial $^{87}Sr/^{86}Sr$ ratios (Fig. 9A). The other two samples have higher $\varepsilon_{Nd}(t)$ values and initial $^{87}Sr/^{86}Sr$ ratios. The plagiogranites have initial $^{87}Sr/^{86}Sr$ ratios ranging from 0.70338 to 0.70444 and initial $^{143}Nd/^{144}Nd$ ratios varying from 0.512897 to 0.513140, with $\varepsilon_{Nd}(t)$ values between +8.2 and +12.9. Seawater alteration may have influenced $^{87}Sr/^{86}Sr$.

Zircon U-Pb Age and Lu-Hf Isotopic Composition

Four plagiogranite samples were selected for zircon U-Pb age determination. The zircons predominantly show long euhedral prismatic shapes with lengths of 120–200 μm and widths of 70–150 μm. In the cathodoluminescence (CL) images, the zircons display broad magmatic oscillatory zoning to weak or no zoning (Fig. 10). Their Th/U ratios range from 0.43 to 1.28. The 20 grains from sample DJ12-17 were plotted on concordia and yielded a concordia age of 121.8 ± 1.0 Ma (mean square of weighted deviates [MSWD] = 1.1; Fig. 10A), while 14 grains from sample DJ12-19 yielded a concordia age of 122.8 ± 1.0 Ma (MSWD = 0. 28; Fig. 10B). For sample DJG13-52, two zircons displayed unusual older ages, which might be inherited zircons, while four zircons showed abnormal younger ages, which might reflect Pb loss. Therefore, analyses that clearly plotted outside of a Gaussian distribution were excluded, and the other 16 spots yielded a weighted mean age of 125.5 ± 1.0 Ma (MSWD = 0.25; Fig. 10C; Table S6). For sample DJG13-96, 23 zircons yielded a concordia age of 125.9 ± 1.0 Ma (MSWD = 0.49; Fig. 10D).

All zircons from samples DJ12-17 and DJ12-19 were analyzed for Hf isotopes.

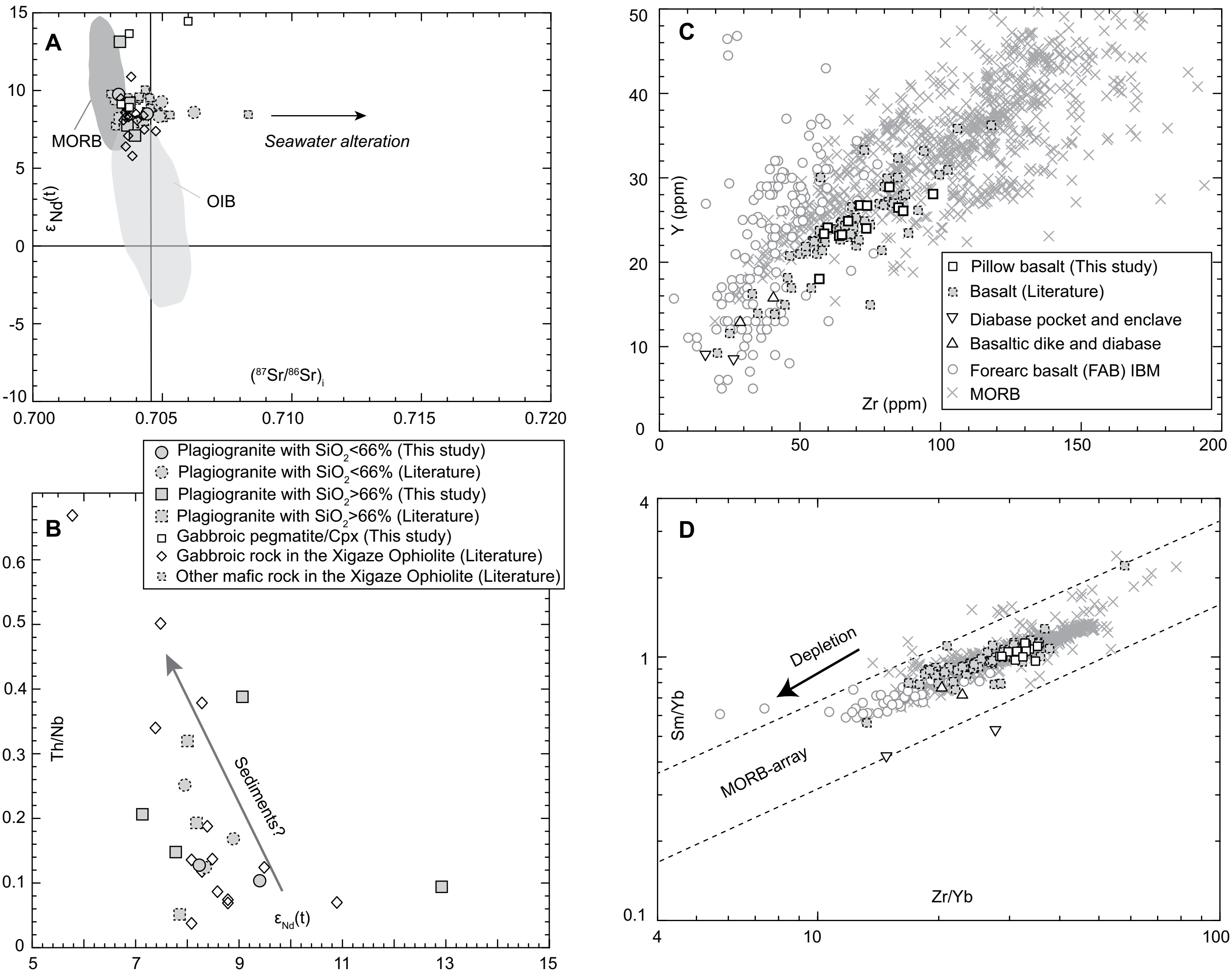

Figure 9. (A) Whole-rock Sr-Nd isotopes of plagiogranite and mafic rock from the Xigaze ophiolite. Fields of mid-ocean-ridge basalt (MORB) and oceanic-island basalt (OIB) are shown (Hofmann, 1997). (B) $\varepsilon_{Nd}(t)$ values vs. Th/Nb for plagiogranites and gabbroic rocks. Data for gabbroic rocks are from Liu et al. (2018); other mafic rocks of the Xigaze ophiolite are from Niu et al. (2006) and Zhang et al. (2016b); plagiogranites are from Zhang et al. (2016b); cpx—clinopyroxene. (C, D) Zr vs. Y, and Zr/Yb vs. Sm/Yb for basalt and diabase. Note that Zr/Y and Zr/Yb ratios for Xigaze ophiolite basalts are higher than Izu-Bonin-Mariana (IBM) forearc basalts, but they are similar to MORB, indicating derivation from a more fertile mantle source. Data sources: basalts in the Xigaze ophiolite are the same as Figure 7; forearc basalts are from Ishizuka et al. (2011, 2018) and Reagan et al. (2010, 2017); global MORB values are from Gale et al. (2013).

Twenty grains of sample DJ12-17 displayed a range of initial $^{176}Hf/^{177}Hf$ ratios from 0.283020 to 0.283164, and high positive $\varepsilon_{Hf}(t)$ values of +11.0 to +15.9 (Fig. 10E; Table S7). Their Hf depleted mantle model (T_{DM}) ages range from 377 to 141 Ma. Sample DJ12-19 yielded 14 reliable Hf data points with initial $^{176}Hf/^{177}Hf$ ratios ranging from 0.283056 to 0.283174. They also showed positive $\varepsilon_{Hf}(t)$ values of +12.6 to +16.4 and young Hf T_{DM} model ages of 296–129 Ma.

DISCUSSION

Below, we used our new and compiled data to address three important questions: (1) When and for how long did seafloor spreading happen in the Xigaze ophiolite? (2) How were mafic and felsic magmas generated? (3) How similar or dissimilar were the processes that formed the Xigaze ophiolite to those that formed the Izu-Bonin-Mariana forearc? These three questions are explored in this order below.

Age and Duration of Seafloor Spreading in the Xigaze Ophiolite

Although plagiogranites are minor components of ophiolites, they are frequently used for dating ophiolite magmatic activities because they usually contain zircons for U-Pb geochronology (e.g., Singh et al., 2017). Four plagiogranite samples from three different locations (locations A, C, D in Fig. 3B) yielded zircon U-Pb ages of 121.8 ± 1.0 Ma, 122.8 ± 1.0 Ma,

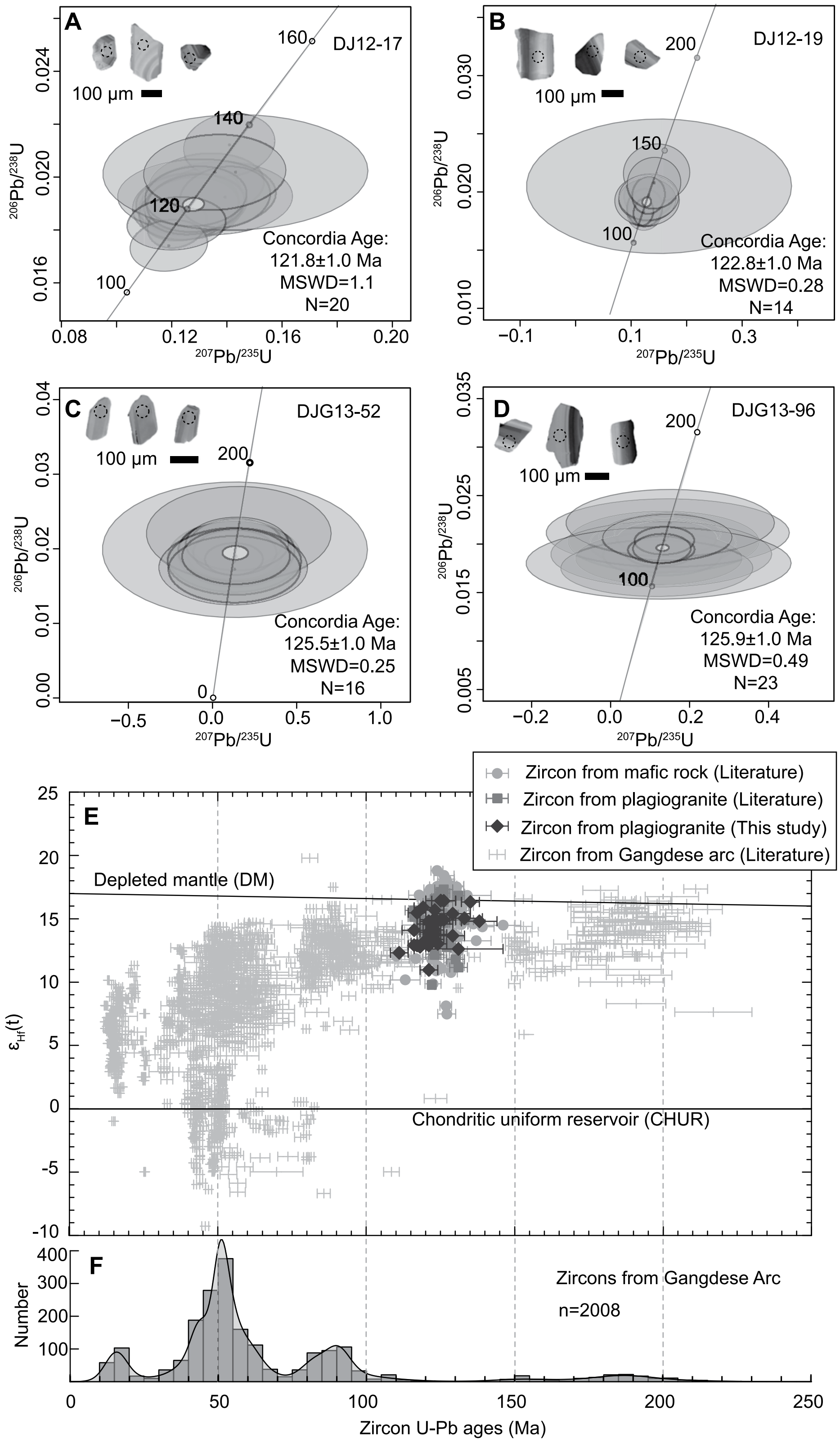

Figure 10. (A–D) Zircon U-Pb concordia plots for four plagiogranite samples (DJ12-17, DJ12-19, DJG13-52, DJG13-96) and representative cathodoluminescence images of zircons. MSWD—mean square of weighted deviates. (E) Plot of $\varepsilon_{Hf}(t)$ vs. U-Pb age of zircons from plagiogranite and mafic rock in the Xigaze ophiolite. (F) Plot of $\varepsilon_{Hf}(t)$ vs. zircon U-Pb ages of Gangdese arc. Data for mafic rock and plagiogranite are from Dai et al. (2013); Liu et al. (2016); and Zhang et al. (2016b). Data for the Gangdese arc are from Chu et al. (2011); Guan et al. (2012); Guo et al. (2013); Huang et al. (2016); Ji et al. (2009, 2012); Ma et al. (2013); Pan et al. (2016); Wang et al. (2015); B. Xu et al. (2017); Xu et al. (2015); Yang et al. (2016); Zhang et al. (2010); and Zhu et al. (2011).

125.5 ± 1.0 Ma, and 125.9 ± 1.0 Ma, respectively (Figs. 10A–10D). These ages are similar to those previously reported from plagiogranites from Deji to Pengcang with ages ranging from 123.3 ± 1.5 Ma to 129.6 ± 1.5 Ma (Dai et al., 2013; Zhang et al., 2016b).

In the Xigaze ophiolite, there are plenty of radiometric ages from mafic rocks, including isotropic gabbro, diabase sill, and various gabbroic/diabase dikes intruded into both the crustal and mantle sections. These ages range from 124 ± 1.6 Ma to 130 ± 1.3 Ma (Fig. 3B; Bao et al., 2013; Dai et al., 2013; Liu et al., 2016; Zhang et al., 2016b), which are comparable to those of the plagiogranites. These ages indicate that both mafic and felsic intrusive rocks in the Xigaze ophiolite were generated in the Early Cretaceous, i.e., 130.0–121.8 Ma (Fig. 10E). However, Middle–Late Jurassic ages (174.0 ± 3.8 Ma and 169.1 ± 1.9 Ma) from two gabbro samples from the Dazhuqu and Jiding massifs have been reported recently in the Xigaze ophiolite (X. Wang et al., 2018), which are interpreted as products of an earlier stage of igneous activity in the Neo-Tethyan Ocean, unrelated to the Early Cretaceous magmatism. Most ages suggest that the duration of Xigaze ophiolite magmatic activity during the Early Cretaceous stage was ~10 m.y., consistent with the conclusions of Hu and Stern (2020).

Petrogenesis of Mafic and Felsic Dikes and Pillow Basalt in the Xigaze Ophiolite

Flux Melting of Depleted Mantle to Generate Gabbroic Pegmatite and Basaltic and Diabase Dikes

Clinopyroxenes from gabbroic pegmatite have lower Al_2O_3 and TiO_2 contents (Figs. S2B and S2C), indicating that their parental melts were derived from a more depleted mantle source than that of the common mafic rocks in the Xigaze ophiolite. The moderate initial $^{87}Sr/^{86}Sr$ ratios and high $\varepsilon_{Nd}(t)$ values also indicate a depleted mantle source. The low Sr contents and thus negative anomaly of clinopyroxenes (Fig. 8A) indicate the crystallization of plagioclase.

REE and trace-element patterns of clinopyroxenes from the gabbroic pegmatite indicate that they are depleted in HFSEs (Figs. 7A and 8A), implying that their parental melts were generated from refractory mantle. HFSEs, including Zr and Y, are incompatible elements that concentrate in magma until zircon begins to precipitate. Clinopyroxene megacrysts are near-liquidus phases precipitated from melts (Akinin et al., 2005). Therefore, Zr and Y contents and thus Zr/Y ratios of clinopyroxene probably record source compositions of parental melts. In the Zr versus Y diagram (Fig. 11A), the majority of our clinopyroxenes plot within the field of clinopyroxenes of late gabbroic rocks from the Oman ophiolite (Yamasaki et al., 2006). Zr concentrations and Zr/Y ratios of our clinopyroxenes are low and lie between the corresponding range of clinopyroxenes from ordinary arc igneous rocks and boninites, indicating that their parental melts were derived from a high degree of partial melting of a depleted source.

In order to obtain further information on their source, we calculated the REE concentrations of melts in equilibrium with clinopyroxenes, and the partition coefficients of REE between clinopyroxenes and hydrous silicate melts were employed (Gaetani et al., 2003). This method assumes that the clinopyroxene compositions were not modified by postcrystallization processes. The uniformity of REE compositions of our clinopyroxenes and the lack of mineralogical zoning indicate that they did not experience significant postcrystallization compositional modification. Therefore, REE concentrations of these clinopyroxenes preserve their original compositions and can be applied to calculate REE contents of the melts from which they formed. Although Mg# values of clinopyroxenes vary, there are no significant differences in REE contents against Mg# values. Therefore, all the clinopyroxene compositions were used to calculate their equilibrium melts. Only one analysis showed significantly higher REE contents of calculated melt than the others (Figs. 7C and 7D), which might reflect mineral inclusions; thus, it is excluded from further discussion. The calculated results indicate that melts in equilibrium with clinopyroxenes in most gabbroic pegmatite samples have REE contents distinctly lower than those of modern MORB, especially for HREE contents (Fig. 7C). Such characteristics are similar to those of low-K island-arc tholeiites in Tonga (Ewart and Hawkesworth, 1987; Meffre et al., 2012) and in the South Sandwich Islands (Fig. 7D; Pearce et al., 1995), indicating that the melt might be equivalent to island-arc tholeiite. LREE and HREE patterns of the calculated melts resemble those of depleted lavas in the Xigaze ophiolite (Fig. 7C; Chen and Xia, 2008; Dai et al., 2013; Dubois-Côté, et al., 2005; Li et al., 2012; Niu et al., 2006; Zhang et al., 2016b) and overlap with those of V2-type extrusive rocks in the Oman ophiolite (Fig. 7D; Godard et al., 2003). The depleted source of calculated melts is also indicated by low Nd/Yb ratios and Yb contents. In the plot of $(Nd/Yb)_N$ versus Yb_N (Fig. 11B), our calculated melts in equilibrium with clinopyroxenes display features similar to those of late gabbroic rocks in the Oman ophiolite (Yamasaki et al., 2006) and the depleted lavas and dikes of the Xigaze ophiolite. Both V2-type extrusive rocks (Godard et al., 2003) and late gabbroic rocks (Yamasaki et al., 2006) in the Oman ophiolite are proposed to have been generated above a subduction zone. These observations indicate that the parental melts of the gabbroic pegmatites were derived from fluid-enhanced melting of a depleted mantle source.

Basaltic dike and diabase enclave/pocket samples are characterized by LILE enrichment and significant HFSE depletion, especially negative Nb and Ta anomalies (Fig. 8D), suggesting that they reflect flux melting of a depleted mantle. Their depleted mantle source is also supported by low Zr and Y contents (Fig. 9C).

The formation of diopside megacrysts in the gabbroic pegmatite suggests that their equilibrium melts were rich in H_2O and Ca (Beard and Scott, 2018; Harlov et al., 2014; Santosh et al., 2010), and they also suggest slow cooling. The inferred hydrous parental melts are consistent with the textural and geochemical characteristics of amphiboles in the gabbroic pegmatite. Amphiboles occur as euhedral grains, anhedral blebs, or coronas around clinopyroxene and plagioclase at their grain boundaries (Figs. 6D and 6E). The textural characteristics resemble those of hydrothermal amphiboles in oceanic gabbros (Coogan et al., 2001). Commonly, magmatic amphiboles are characterized by lower SiO_2 (<46 wt%) and higher Al_2O_3 (>10 wt%) contents (Coogan, 2003). However, all amphiboles from the gabbroic pegmatite have higher SiO_2 (>46 wt%) and lower Al_2O_3 (<10 wt%) contents (Fig. S2D), as expected for hydrothermal amphiboles (Coogan, 2003; Coogan et al., 2001). The above characteristics are also similar to those of amphiboles from the Purang gabbronorite (Liu et al., 2014), which are considered to have formed during seawater alteration at low temperature. However, the estimated temperature from amphiboles of the gabbroic pegmatite here ranges from 703 °C to 846 °C (Table S3), indicating that the formation of these minerals was not associated with seawater alteration.

Amphiboles generated in the mantle wedge above subduction zones are characterized by depletion in Nb and high Ti/Nb and Zr/Nb ratios (Coltorti et al., 2007). Amphiboles from the gabbroic pegmatite plot within the fields of suprasubduction zone amphiboles in the Nb versus Ti and Zr/Nb versus Ti/Nb diagrams (Figs. 11C and 11D). REE and trace-element patterns of amphiboles from the gabbroic pegmatite resemble those of amphiboles from Ichinomegata, Japan (Fig. 7B). Amphiboles from Ichinomegata peridotite xenoliths represent the melts and fluids from mantle metasomatism in a subduction setting (Coltorti et al., 2007). These observations suggest that amphiboles of the gabbroic pegmatite inherited their signature from fluids extracted from the subducted slab (Coltorti et al., 2007).

Both petrographic and geochemical characteristics of clinopyroxenes and amphiboles suggest that the gabbroic pegmatite formed from hydrous high-SiO_2 island-arc tholeiite melts. Fluids were possibly derived from dehydration of the subducted slab. Late gabbroic rocks of the Oman ophiolite, with geochemical characteristics (Figs. 7A and 8A) similar to those of the gabbroic pegmatites, have been considered to represent a suprasubduction zone setting (Yamasaki et al., 2006). Therefore, the late stages of gabbroic pegmatite dike and basaltic dike and diabase enclave/pocket emplacement were generated from flux melting of a depleted harzburgite that had undergone previous melt extraction.

Hydrous Melting of Amphibolite in the Metamorphic Sole to Form Plagiogranites

Even though volumetrically minor in the oceanic crust and ophiolite complexes, petrogenesis of plagiogranites is an intriguing topic. Three major models have been proposed to explain plagiogranite petrogenesis: (1) fractional crystallization of basaltic melts (Aldiss, 1981; Dilek and Thy, 2006); (2) partial melting of metasomatized gabbroic rocks or amphibolites (Gillis and Coogan, 2002; Koepke et al., 2007; Pedersen and Malpas, 1984); and (3) liquid immiscibility (Dixon and Rutherford, 1979). Liquid immiscibility for the Xigaze plagiogranite can be ruled out because the associated immiscible Fe-rich liquid (as Fe-rich mafic unit) of the Xigaze ophiolite is absent.

If plagiogranites in the Xigaze ophiolite were generated by fractional crystallization from basaltic melts, they should show geochemical similarities to mafic rocks of the crustal section in the Xigaze ophiolite. Most plagiogranites do not plot along the trend constrained by the aforementioned units of the Xigaze ophiolite on the major- and trace-element variation diagrams (Figs. S3 and S4). However, the plagiogranites define their own fields, distinct from those of the mafic rocks and clearly indicating that they did not form by simple fractional crystallization.

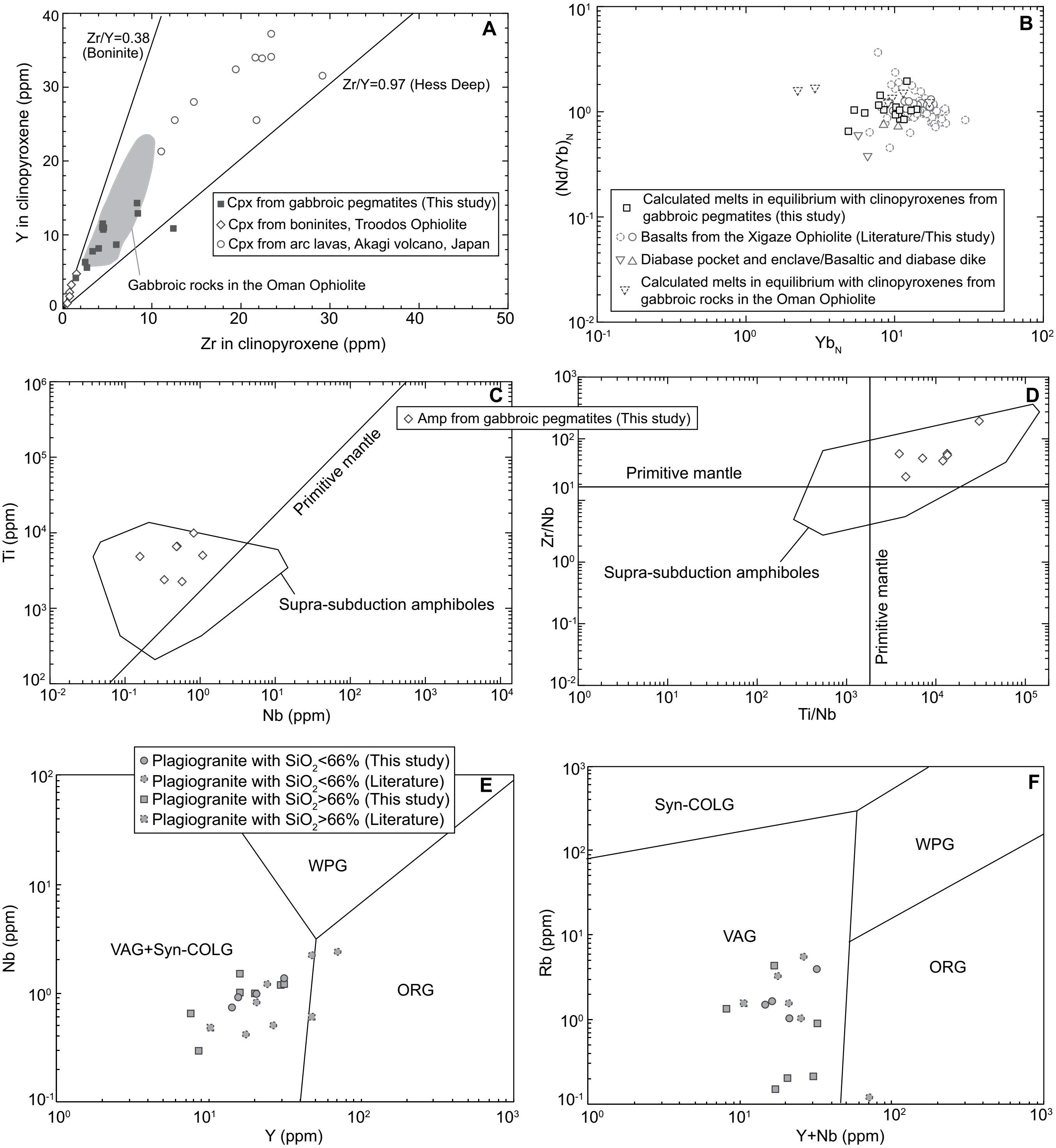

Figure 11. (A) Zr vs. Y concentrations of clinopyroxenes (cpx). Field of Oman late gabbroic rocks is from Yamasaki et al. (2006); boninites of the Troodos ophiolite are from Sobolev et al. (1996); arc lavas of Akagi volcano, Japan, are from Kobayashi and Nakamura (2001); oceanic gabbros at fast-spreading center of Hess Deep are from Coogan et al. (2002). (B) Chondrite-normalized Nd/Yb ratios in the calculated melts in equilibrium with clinopyroxenes of our samples and the late gabbroic rocks in the Oman ophiolite (Yamasaki et al., 2006). Please see detailed calculation in the text. For comparison, previously published basalts of the Xigaze ophiolite are also plotted. Basalt data source are the same as Figure 7. Chondrite-normalized values are from Sun and McDonough (1989). (C, D) Ti vs. Nb, and Zr/Nb vs. Ti/Nb diagrams for amphiboles from the gabbroic pegmatite. Fields of suprasubduction amphiboles are from Coltorti et al. (2007). (E, F) Tectonic discrimination diagrams for the Xigaze plagiogranite: (E) Nb vs. Y and (F) Rb vs. Y + Nb (Pearce et al., 1984). VAG—volcanic-arc granite; ORG—oceanic-ridge granite; WPG—within-plate granite; Syn–COLG—syncollisional granite.

Some geochemical indicators can distinguish fractional crystallization and partial melting processes. First, experimental studies show that low TiO_2 contents (usually <1 wt%) observed for plagiogranites are produced through partial melting of low- TiO_2 oceanic gabbros (Koepke et al., 2004). Koepke et al. (2007) further proposed that the TiO_2 content of plagiogranite effectively discriminates between hydrous partial melting of oceanic gabbros and fractional crystallization of MORB. They showed a line that represents the minimum TiO_2 values of SiO_2-enriched melt generated by differentiation of a MORB-type parental magma in tholeiitic systems in the SiO_2-TiO_2 diagram (Fig. S5B). Most Xigaze ophiolite plagiogranites have low TiO_2 contents, which overlap with the experimental melts derived from the hydrous melting of oceanic gabbros (Fig. S5B). These observations suggest that Xigaze ophiolite plagiogranites formed by hydrous melting of gabbros rather than by extended fractional crystallization of tholeiitic MORB melts. This was also proposed by Zhang et al. (2016b) because the plagiogranites have low TiO_2 and Sr-Nd-Hf isotopes indistinguishable from those of mafic dikes.

Second, some Xigaze ophiolite plagiogranites have lower REE contents than those of associated mafic rocks (Fig. 7E). Brophy (2008) proposed that REE-SiO_2 systematics can discriminate the above two hypotheses for plagiogranite origin, because most common minerals, especially hornblende, play different roles in the two processes. Partition coefficients of REE between hornblende and liquid increase significantly when liquid SiO_2 contents increase, and so REEs should change from incompatible to compatible elements (Brophy, 2008). These observations, in a combination with the fact that hornblende is a major crystallizing and melting mineral during gabbro melting, while hornblende crystallization is negligible during basalt fractionation, led Brophy (2008) to propose that partial melting of mafic amphibolite should yield constant or decreasing La and constant Yb abundances with increasing liquid SiO_2 contents. He also inferred that REE contents between related mafic rocks and felsic rocks should be similar in the case of partial melting, whereas fractional crystallization of MORB-like melts should yield steadily increasing La and Yb abundances with increasing SiO_2, and REE contents of felsic rocks should be higher than those of associated mafic rocks. The plagiogranites and mafic rocks in the Xigaze ophiolite have similar contents of La and Yb with increasing SiO_2 contents (Fig. S4). These La-SiO_2 and Yb-SiO_2 patterns are consistent with the patterns of hydrous melting of mafic amphibolite (Brophy, 2008), and they clearly differ from the predicted patterns from MORB fractional crystallization.

Sr and Nd isotopic compositions of plagiogranites further constrain their source and the processes by which they formed. There are two observations indicating that an enriched subduction component was involved in plagiogranite generation: (1) The negative correlation between Th/Nb ratios and $\varepsilon_{Nd}(t)$ (Fig. 9B) indicates that sediment melts might have been added because sediments typically have high Th/Nb; (2) most plagiogranites have more radiogenic Sr isotopes (with an initial $^{87}Sr/^{86}Sr$ ratio up to 0.70451) and plot to the right of the MORB field (Fig. 9A). Therefore, plagiogranites in the Xigaze ophiolite are likely to have been generated by partial melting of altered mafic amphibolite, and the felsic melts migrated upward and intruded into the mantle peridotites. Taking the regional geological setting into account, the ideal source candidate is amphibolite in the metamorphic sole (Guilmette et al., 2009), which has been reported at Bainang close to our study area (Fig. 3B). Considering that amphibolite also has lower TiO_2, it was quite likely the source of the plagiogranite, similar to that in the Oman mantle (Cox et al., 1999). Commonly, amphibolites are strongly deformed, with high-temperature foliation, and they occur within the ophiolitic mélange. The metamorphic sole is considered to mark the top of the shallow subduction zone. The protoliths of these rocks are considered to be MORBs (Guilmette et al., 2009).

Decompression Melting of Relatively Fertile Mantle to Produce Pillow Basalt

Most Xigaze ophiolite pillow basalts display LREE-depleted patterns similar to that of N-MORB (Fig. 7E). In the plots of Zr/Yb versus Sm/Yb and Zr versus Y, all our basalts and previously published basalts from the Xigaze ophiolite plot in the "MORB array" (Fig. 9D) and overlap with global MORB (Fig. 9C). However, the pillow basalts and other published basalts display pronounced depletion of Nb and Ta, and some enrichment of LILEs, resembling those of Izu-Bonin-Mariana forearc basalts (Fig. 8F). In this context, the generation mechanism of the Xigaze ophiolite basalts is similar to Izu-Bonin-Mariana forearc basalts; that is, the partial melting was mainly caused by decompression as the contribution of fluids derived from the sinking slab during this stage was limited. Xigaze ophiolite basalts have higher Zr/Y and Zr/Yb ratios than those of Izu-Bonin-Mariana forearc basalts, indicating that they may have been generated from a more fertile mantle source compared to Izu-Bonin-Mariana forearc basalts (Figs. 9C and 9D).

SUBDUCTION INITIATION RECORDED IN THE XIGAZE OPHIOLITE AND COMPARISON WITH IZU-BONIN-MARIANA FOREARC

The Xigaze Ophiolite Was Generated in a Forearc Setting

As discussed earlier herein, there are several different models for the tectonic setting of the Yarlung Zangbo ophiolite. An important reason for this controversy is that most studies are based on a certain part of the ophiolite instead of the entire ophiolite belt, and they have rarely considered the regional geological setting. In this section, we combine all the available data sets to better constrain the tectonic setting and geodynamic evolution of the Xigaze ophiolite.

The tectonic setting of the Xigaze ophiolite can be recognized by geochemical data. On the N-MORB–normalized multi-element variation diagram, most pillow basalts display affinity with Izu-Bonin-Mariana forearc basalt, whereas gabbroic pegmatites, basaltic dikes and diabase enclaves/pockets, and plagiogranites exhibit depletion of most HFSEs, including negative Nb and Ta anomalies and LILE enrichment (Figs. 8C–8F). These observations indicate that these igneous rocks may have formed in a suprasubduction zone setting. Furthermore, the plagiogranites show a volcanic-arc granite affinity on the tectonic discrimination diagrams of Nb versus Y and Rb versus Nb + Y (Figs. 11E and 11F; Pearce et al., 1984). The similar ages between plagiogranites and the other ophiolite units as well as their proximity suggest that they formed in the same tectonic setting (Fig. 10E). The subduction-related setting of the above lithologies also indicates that the Xigaze ophiolite was generated in the same setting. This inference is consistent with other lines of evidence, including: (1) the low $\delta^{26}Mg$ values of rodingites in the Xigaze ophiolite, which might have been caused by subducted carbonates (Dai et al., 2016); (2) the typical suprasubduction zone characteristics of chromitites and peridotites in the Zedang and Luobusa ophiolites in the eastern part of the Yarlung Zangbo ophiolite (Xiong et al., 2016; Griffin et al., 2016); and (3) the Re-Os isotope and highly siderophile element (Os, Ir, Ru, Pt, Pd, and Re) geochemical data of Yarlung Zangbo ophiolite peridotites, suggesting that the mantle lithosphere was pervasively infiltrated by S-saturated basaltic melts during Neo-Tethyan subduction (Xu et al., 2020).

A complex intra-oceanic arc–back-arc model has been proposed for the Yarlung Zangbo ophiolite (Hébert et al., 2012), but it fails to explain several important observations. For example, where is the associated magmatic

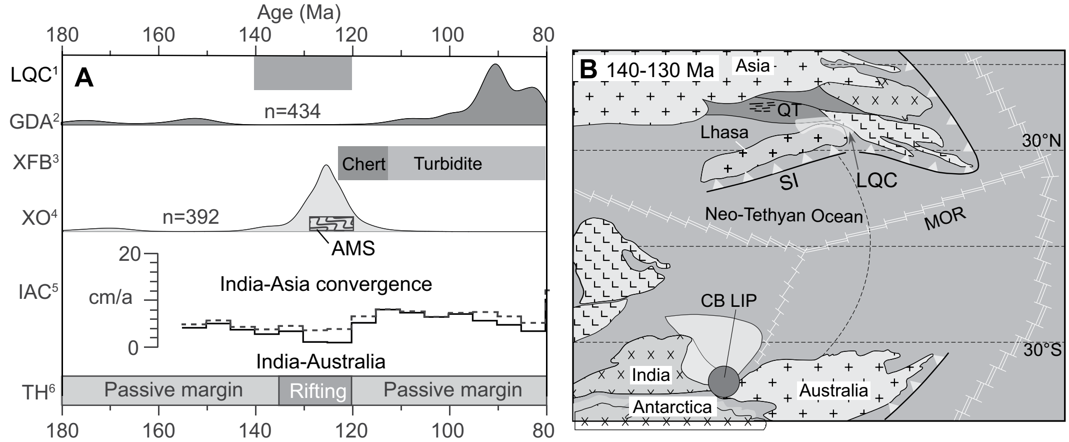

Figure 12. (A) Compilation of geochronological ages of related geological units and tectonic events (revised from Metcalf and Kapp, 2019) and (B) paleogeographic reconstruction of the southern Tibetan Plateau (revised from Zhu et al., 2013). 1—LQC, timing of Lhasa-Qiangtang Collision (LQC) from Zhu et al. (2013) and Kapp et al. (2007). 2—GDA, ages of Gangdese arc (GDA) from Chu et al. (2011); Guo et al. (2013); Ji et al. (2009); Ma et al. (2013); Pan et al. (2016); Xu et al. (2015); and Zhu et al. (2011). 3—XFB, lithology and ages of the Xigaze forearc Basin (XFB) from Dai et al. (2015); Wang et al. (2017); Wang et al. (2012); and Wu et al. (2010). 4—XO, ages of the Xigaze ophiolite from Bao et al. (2013); Dai et al. (2013); Liu et al. (2016); Li et al. (2009); Wang et al. (2018); and Zhang et al. (2016b); amphibolite metamorphic sole (AMS) ages are from Guilmette et al. (2009). 5—India-Eurasia convergence (IAC) rate at the eastern syntaxis (dashed black) and the western syntaxis (solid black) from Gibbons et al. (2015). 6—Tethyan Himalaya (TH) strata ages and events, with Cretaceous rifting from Zhu et al. (2009) and Zhou et al. (2017). SI—subduction initiation; MOR—mid-ocean ridge; CB LIP—Comei-Bunbury large igneous province; QT—Qiangtang.

arc? In contrast, the following four geological observations indicate that the Xigaze ophiolite was generated in a forearc: (1) Forearc basin sediments were deposited directly on the Xigaze ophiolite immediately after the cessation of extension (Fig. 12A; An et al., 2014; Dai et al., 2015; Wang et al., 2017), implying that the ophiolite is the basement of the forearc basin. (2) Indistinguishable paleolatitude estimates between the Lower Cretaceous sedimentary rocks overlying the Xigaze ophiolite and the Gangdese arc (Huang et al., 2015) suggest that the ophiolite formed close to the Asian continental margin. (3) The occurrence of ultradepleted harzburgite has been documented (Zhang et al., 2017), which is characteristic of forearc peridotite. (4) The associated magmatic arc is the Cretaceous Gangdese batholith and related volcanic rocks, which lie well to the north of the Yarlung Zangbo ophiolite and firmly establish the Yarlung Zangbo ophiolite as representing forearc lithosphere.

Forearc Magmatic Evolution in the Xigaze Ophiolite During Subduction Initiation and Comparison with Izu-Bonin-Mariana Forearc

There are some differences between the sequence of the Xigaze ophiolite and the Izu-Bonin-Mariana forearc. First, most basalts in the Xigaze ophiolite show less depleted mantle sources than that of Izu-Bonin-Mariana forearc basalt, albeit some are similar (Figs. 9C and 9D). Second, the Xigaze ophiolite lacks abundant boninites, although some have been documented. Dai et al. (2013) reported that boninitic dikes in the Xigaze ophiolite gave U-Pb zircon ages of ca. 125 Ma, and other boninites were also reported from the Xigaze area (Chen et al., 2003; Malpas et al., 2003; Dubois-Côté et al., 2005). Furthermore, Zhong et al. (2019) reported forearc basalt–like and boninitic mafic rock in the western Yarlung Zangbo suture zone. Indeed, boninites are not always a necessary component for a forearc sequence during subduction initiation (Yu et al., 2020).

Do the above differences from the Izu-Bonin-Mariana forearc indicate that the Xigaze ophiolite was not generated during subduction initiation? The answer to this question mainly depends on the magmatic expression of subduction initiation. The subduction initiation magmatic sequence begins with upwelling of ambient mantle. In Izu-Bonin-Mariana, this was asthenospheric mantle that generated forearc basalts by decompression melting. Subduction initiation magmatism later produces arc-like lavas from fluid-induced partial melting of depleted harzburgitic residue (Whattam and Stern, 2011). For the Xigaze ophiolite, most basalts are similar to Izu-Bonin-Mariana forearc basalts, but they are relatively enriched, while later basaltic and gabbro pegmatite dikes and diabase enclaves/pockets are more depleted melts resulting from subsequent partial melting of harzburgite triggered by fluids from the sinking slab. In addition, based on the association of gabbroic pegmatite and plagiogranite and their field relations, we infer that these melts were coeval (Fig. 5J). Mafic and felsic dikes intruded the mantle contemporaneously, although they had different sources. The association of these types of rocks suggests coeval intrusion of melts from both sources into the same domains within the upper mantle, indicating that they were generated in the same tectonic setting. Therefore, the Xigaze ophiolite records one transient Neo-Tethyan subduction initiation event in the Early Cretaceous (130–120 Ma). A similar conclusion was recently reached by Hu and Stern (2020), who argued that the Yarlung Zangbo ophiolite formed during an important episode of subduction initiation in Early Cretaceous time. Compared to Izu-Bonin-Mariana forearc igneous rocks, the Xigaze ophiolite may have had more variable melting processes, magmatic composition, and evolution.

Why were most basalts in the Xigaze ophiolite derived from more fertile mantle than that responsible for Izu-Bonin-Mariana forearc basalt? Subduction initiation decompression melting will involve ambient mantle flowing in from beneath the overriding plate; in the case of Izu-Bonin-Mariana, the ambient mantle beneath the overriding plate was depleted oceanic asthenosphere (Ishizuka et al., 2011, 2018), but this was not available for the Xigaze subduction initiation. Instead, more fertile subcontinental mantle flowed in from beneath the Lhasa block or may have come from greater depths, as indicated by the abundance of diamonds in peridotites from different ophiolitic massifs along the entire Yarlung Zangbo suture zone (Yang et al., 2014; Griffin et al., 2016). This inference is also supported by accretion of lherzolite at the Zedang ophiolite in the eastern Yarlung Zangbo suture zone (Fig. 4E). The lherzolite was proposed to be a residue after moderate decompression melting of the upwelling asthenosphere during the formation of magma products, i.e., the diabase dike that intruded into the harzburgite, between 130 and 120 Ma (Xiong et al., 2016; Fig. 4E). In the Xigaze ophiolite, the lherzolite is located in basal sections, while the harzburgite is close to the ophiolitic crustal sections (Nicolas et al., 1981), implying that the lherzolite may have been closer or even originated from the asthenosphere. The harzburgite was interpreted to have undergone a more complex metasomatic history resulting from Neo-Tethyan subduction since as early as the Jurassic (Xiong et al., 2016).

The Jurassic subduction of the Neo-Tethys beneath the southern Lhasa block has been proposed on the basis of both the Early Jurassic magmatic rocks in the Gangdese arc (Chu et al., 2006) and the scattered Middle–Late Jurassic ophiolites in the Yarlung Zangbo suture zone (Chan et al., 2015), including the Xigaze ophiolite (Wang et al., 2018). Early Jurassic intrusive and volcanic rocks in the Gangdese arc display arc geochemical characteristics with high positive zircon $\varepsilon_{Hf}(t)$ values suggesting a juvenile mantle contribution. Therefore, Early Jurassic magmatism is interpreted as an early product of the Neo-Tethyan subduction (Chu et al., 2006; Ji et al., 2009; Kang et al., 2014). However, Zhu et al. (2011) proposed that Early Jurassic magmatic rocks were generated in a back-arc extensional region associated with the southward subduction of the Bangong-Nujiang Tethyan ocean. Middle–Late Jurassic magmatism is limited in the Gangdese arc, but the occurrence of the Late Jurassic Zedang arc (ca. 160–150 Ma) in the eastern Yarlung Zangbo suture zone supports Jurassic subduction (Fig. 13A; McDermid et al., 2002; Zhang et al., 2014). In addition, the Zedang arc and the Middle–Late Jurassic ophiolite were generated during a lull in Gangdese arc magmatism (Fig. 12A). Therefore, they were proposed to have formed in a marginal ocean basin caused by forearc extension along the southern margin of the Lhasa block during trench retreat (Metcalf and Kapp, 2019; Kapp and DeCelles, 2019). The newly discovered Xiazha Formation (with a single-zircon peak age of 159–157 Ma), located in the mélange on the south side of the Cretaceous ophiolite, may have formed in the forearc marginal basin proximal to the Zedang arc, providing more evidence for Jurassic subduction along the southern Asian margin (Metcalf and Kapp, 2019). Taking into account the current distribution of the Zedang arc (north of the ophiolite) and Xiazha Formation (south of the ophiolite) and their restricted outcrops, Jurassic forearc crust may have been removed by subduction erosion, while the depleted mantle (probably mainly harzburgite) may have been preserved (Fig. 13A). It should be noted that the presence of significant age peaks ranging from 159 to 134 Ma for both sandstone block and matrix in the mélange of the central Yarlung Zangbo suture zone (Metcalf and Kapp, 2019) suggests that evidence for the Zedang arc and Xiazha Formation may exist more widely than is currently known. There is much we have to learn about Jurassic igneous and tectonic activity of the Lhasa block and how it influenced Early Cretaceous subduction initiation.

Early Cretaceous subduction initiation reflects the rapid retreat of the Neo-Tethyan oceanic slab as it began to subduct (Fig. 13B). During early subduction initiation, fast rollback of the subducted slab caused upper-plate extension that led to mantle upwelling. Decompression melting of enriched deeper mantle or subcontinental lithospheric mantle accompanied seafloor spreading in the overlying plate and produced Izu-Bonin-Mariana forearc basalt–like oceanic crust underlain by lherzolite. The large proportion of lherzolite in the peridotite (one third of peridotite; Liu et al., 2019; Fig. 3B) suggests the possibility of lherzolite accretion. As the slab sank deeper, fluids from the subducted slab began to cause flux melting of the previously depleted mantle (mainly harzburgite), influenced by subduction probably since the Jurassic, to yield high-SiO_2, depleted melts, including gabbroic pegmatite and basaltic dikes, and diabase envelopes/pockets during late-stage subduction initiation (Fig. 13B). At the same time, the metamorphic sole was subjected to partial melting, leading to the formation of plagiogranites.

We do not know if Early Cretaceous Xigaze subduction initiation was spontaneous or induced. Some other Early Cretaceous geological events may have been linked to this subduction initiation event. First, diachronous collision between the Lhasa and Qiangtang blocks occurred at ca. 140–120 Ma (Kapp et al., 2007; Zhu et al., 2013), beginning in the east and migrating west with time (Fig. 12). If the Neo-Tethys continued to converge with Asia, this collision may have provided a far-field force to induce failure of the southern continental margin of the Lhasa block and subduction initiation along that margin. Second, rifting ca. 138–130 Ma in eastern Gondwana (Zhu et al., 2009; Zhou et al., 2017), which led to opening of the Indian Ocean and the northward drift of India, might have played a role (Fig. 12B). Rifting caused by the Comei-Bunbury plume might have pushed the Neo-Tethyan lithosphere northward to induce subduction initiation along the Asian margin. Third, the Zedang arc may have formed in an oceanic marginal basin. In combination, both the Lhasa-Qiangtang collision and the eastern Gondwana breakup, and perhaps the accretion of the Zedang arc, may have provided the force needed for Early Cretaceous subduction initiation beneath the southern margin of Asia. This subduction initiation episode is also supported by the coeval formation of a garnet-amphibolite metamorphic sole in the subduction mélange (Guilmette et al., 2009). Actually, the entire Yarlung Zangbo ophiolite reflects this stage of coeval magmatism (Dai et al., 2013; Zhang et al., 2016a), implying a near-synchronous episode of seafloor spreading associated with subduction initiation along the entire length of the system. We suggest that subduction initiation was induced by a far-field tectonic force caused by both the Lhasa-Qiangtang collision and the eastern Gondwana rifting, but more research is needed to answer the question of what caused Early Cretaceous subduction initiation along the southern margin of the Lhasa block.

In order to better reconstruct Early Cretaceous subduction initiation along the southern Lhasa margin, we compiled information about the temporal evolution of regional magmatic activity, especially for the Gangdese arc (Figs. 10F and 12A). Based on geochronological investigations, at least two main magmatic episodes related to Neo-Tethyan subduction are identified: ca. 205–152 Ma and ca. 109–80 Ma (Ji et al., 2009). A compilation of published zircon U-Pb ages and Hf isotope data from Gangdese arc igneous rocks indicates that these mostly were derived from juvenile sources (Fig. 10E). A significant gap for such arc magmatism during ca. 130–120 Ma is observed. However, the Xigaze forearc basin contains ca. 130–120 Ma detrital zircons (Wu et al., 2010), suggesting that this stage of magmatism might have occurred in the Gangdese arc. Such magmatism was limited compared to other stages, although mafic-felsic magmatism was dominant in the forearc during this time (Fig. 10E). Such a change in southern Tibet magmatism indicates that the Neo-Tethyan slab did not yet lie beneath the Gangdese arc ca. 130–120 Ma. After ca. 120 Ma, no more magmatism is reported from the Xigaze ophiolite, whereas intense magmatism occurred in the Gangdese arc (Fig. 12A). These observations suggest that a normal subducting slab lay beneath the Gangdese arc. This normal subduction might have increased the India-Asia convergence rate (Fig. 12A; Gibbons et al., 2015), which increased at ca. 120 Ma. Continued subduction of the Neo-Tethys and subsequent exhumation of the Gangdese arc resulted in the development of the Xigaze forearc basin. Therefore, the migration of the locus of magmatism from the forearc area to the Gangdese arc is analogous to the migration of magmatic activity westward away from the trench to the Izu-Bonin-Mariana arc (Figs. 1B and 1C; Ishizuka et al., 2011). The duration of forearc magmatism was ~10 m.y., i.e., slightly longer than

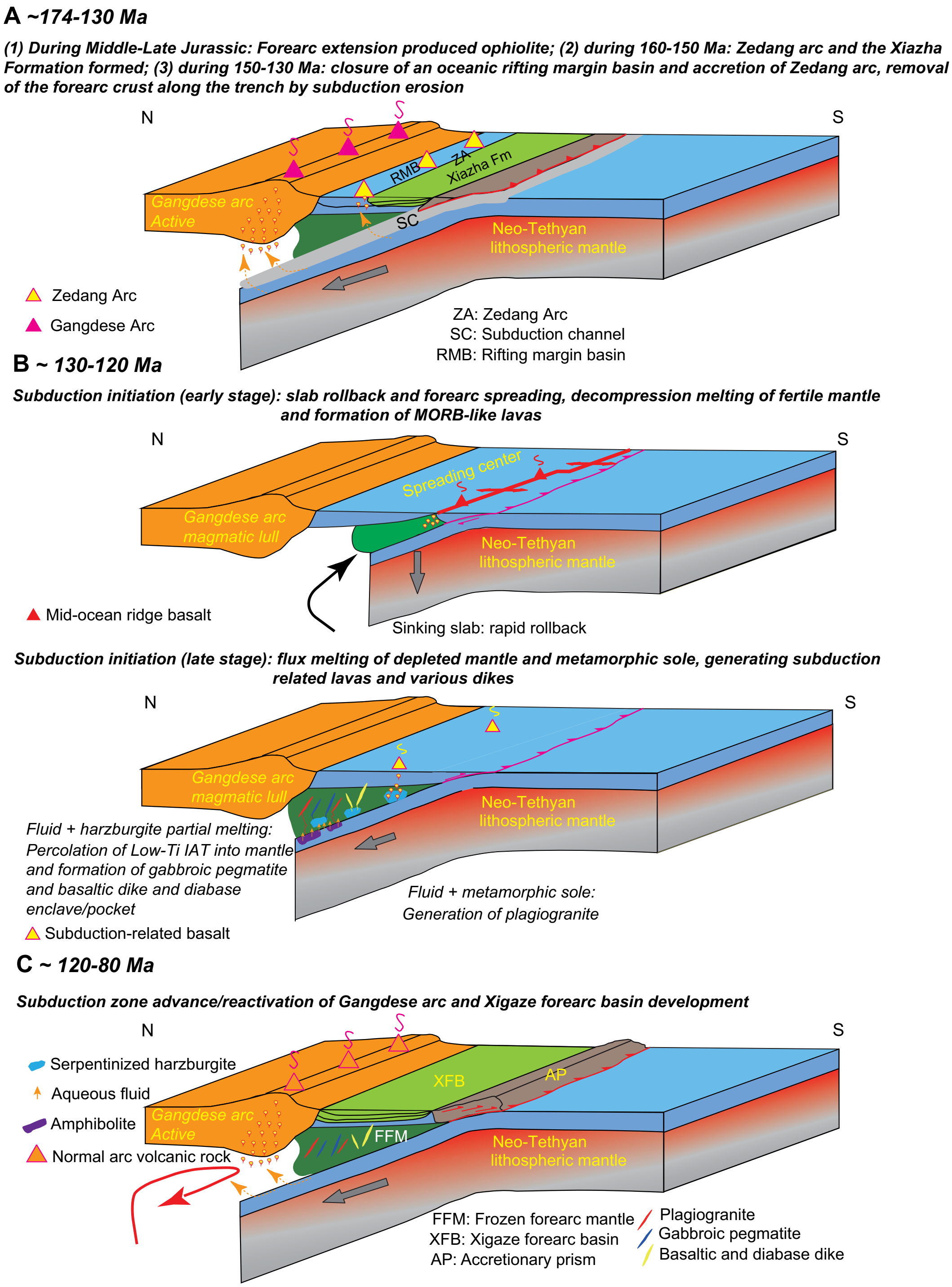

Figure 13. Tectonic model for generation of the Xigaze ophiolite and other Early Cretaceous ophiolites in the Yarlung Zangbo ophiolite. (A) Pre-Cretaceous subduction: Middle–Late Jurassic ophiolite formed by forearc extension; the Zedang arc and Xiazha Formation were generated in a marginal basin; the accretion of the Zedang arc and the subduction erosion of most Jurassic forearc crust (Metcalf and Kapp, 2019). (B) Under far-field tectonic force from both the Lhasa-Qiangtang collision and eastern Gondwana rifting, and possible the accretion of the Zedang arc, northward subduction initiated. During Early Cretaceous subduction initiation, fast rollback of the sinking slab would have induced extension in the upper plate and led to decompression melting of fertile mantle and formation of mid-ocean-ridge basalt (MORB)–like basalts (early stage). As subduction continued, more and more fluids released from the subducted slab would have resulted in flux melting of the depleted mantle and yielded high-SiO_2 depleted melts, finally forming gabbroic pegmatite, basaltic and diabase dikes, and some subduction-related basalts. Similarly, the metamorphic soles also would have undergone partial melting to generate plagiogranite (late stage). IAT—island-arc tholeiite. (C) The locus of magmatism migrated from the forearc to the Gangdese arc, producing abundant volcanic arc and plutonic rocks and allowing the Xigaze forearc basin to develop.

that of the Izu-Bonin-Mariana forearc, which last 7–8 m.y.

GENERATION OF TETHYAN OPHIOLITES AND IMPLICATIONS FOR THE OPHIOLITE CONUNDRUM

The forearc setting noted above for the Xigaze ophiolite could be analogous to that of the Jurassic Albanides-Hellenides ophiolite belt for the following reasons: (1) Both MORB- and suprasubduction zone–type basalts occur in the Xigaze ophiolite (Dai et al., 2013; Dubois-Côté et al., 2005; Li et al., 2012; Zhang et al., 2016b), and these resemble MORB-like basalts and suprasubduction zone–related boninite volcanic rocks in the Pindos (Saccani and Photiades, 2004) and Mirdita ophiolites (Dilek et al., 2008) of Greece; (2) the later-stage mafic dikes with suprasubduction zone geochemical characteristics in the Xigaze ophiolite (Dai et al., 2013; Zhang et al., 2016b) can also be compared with boninitic dikes and gabbroic intrusions in the Pindos (Saccani and Photiades, 2004) and Mirdita ophiolites (Dilek et al., 2008), indicating that they were also derived from partial melting of highly depleted refractory harzburgites. Similarly, two stages of magmatism are also recognized in the Oman–United Arab Emirates ophiolite (Goodenough et al., 2014). Dikes and pillow basalts of the early stage show MORB-like geochemistry, but with small negative Nb and Ta anomalies, suggesting that they were probably generated above a newly initiated subduction zone (MacLeod et al., 2013). Dikes of later stages display significant negative Nb and Ta anomalies and LREE depletion, implying that they formed in a suprasubduction zone setting (Goodenough et al., 2014). The forearc setting subduction initiation mechanism might also have been responsible for generating the aforementioned Tethyan ophiolites, and it can also explain the "ophiolite conundrum" (Moores et al., 2000; suprasubduction zone–type geochemical characteristics versus mid-ocean-ridge seafloor spreading features).

CONCLUSIONS

Based on our new and compiled data from various rocks in the Xigaze ophiolite, the following conclusions are reached:

(1) The geochemical features and calculated REE concentrations of melts in equilibrium with clinopyroxenes indicate that gabbroic pegmatite was derived from hydrous high-SiO_2 island-arc tholeiite melts.

(2) Basaltic dikes and diabase enclaves/pockets show LILE enrichment and significant HFSE depletion, including negative Nb and Ta anomalies, suggesting that they were generated from flux melting of depleted mantle.

(3) Plagiogranite dikes have lower TiO_2 contents but higher Al_2O_3 contents than mafic rocks, while their La and Yb contents are similar, indicating that they were generated by hydrous melting of amphibolite in the metamorphic sole in a suprasubduction zone environment.

(4) Most Xigaze ophiolite pillow basalts exhibit MORB-like REE patterns and similar Zr/Y and Zr/Yb ratios to those of MORB but higher than those of Izu-Bonin-Mariana forearc basalts. They show well-pronounced Nb and Ta depletion that is similar to that of Izu-Bonin-Mariana forearc basalts. These observations imply that the pillow basalts were generated by partial melting of a more fertile mantle source.

(5) Zircon U-Pb age data from the plagiogranites gave Early Cretaceous ages, which are similar to ages of other Xigaze ophiolite mafic rocks. Most ages suggest that the duration of Xigaze ophiolite magmatism was ~10 m.y.

(6) Various different types of rocks can be generated in one transient subduction initiation event along an unknown lithospheric weakness: In the early stage, vertical sinking and fast rollback of the subducted slab leads to strong upper-plate extension, resulting in decompression melting of more fertile mantle to form MORB-like oceanic crust with minor influence from subducted fluids; as subduction initiation progresses, flux melting of previously depleted mantle generates melts with arc-like geochemical signatures, and these intrude the ophiolite to form gabbroic pegmatite and basaltic dikes, and diabase envelopes/pockets. Meanwhile, the metamorphic sole of the ophiolite is partially melted to form plagiogranites.

(7) Both the Lhasa-Qiangtang collision and the breakup of eastern Gondwana triggered Early Cretaceous northward subduction initiation between the Lhasa terrane and the Neo-Tethyan Ocean. The differences in mantle source and magmatic rocks between the Xigaze ophiolite and the Izu-Bonin-Mariana forearc suggest that there is significant diversity in the composition of igneous rocks as a result of variations in subduction initiation processes.

ACKNOWLEDGMENTS

We are grateful to M. Santosh, Ali Polat, Emilio Saccani, Biswajit Ghosh, Shoji Arai, Elizabeth Bell, and Yildirim Dilek for their critical comments and discussions on the early version of this manuscript. Hailong Zhang and Jiawei Zhang are gratefully acknowledged for their assistance in the field and in the mineral major- and trace-element analyses. This study was supported by the National Key Research and Development Program of China (2016YFC0600305), National Natural Science Foundation of China (no. 41872105), and the 111 project (B18048). This is China University of Geosciences–Beijing petrogeochemical contribution PGC-201555 and University of Texas at Dallas geosciences contribution 1369. The data reported in this paper are available as supporting information (see text footnote 1).

REFERENCES CITED

Aitchison, J.C., Davis, A.M., Liu, J., Luo, H., Malpas, J.G., McDermid, I.R.C., Wu, H.Y., Ziabrev, S.V., and Zhou, M.F., 2000, Remnants of a Cretaceous intra-oceanic subduction system within the Yarlung–Zangbo suture (southern Tibet): Earth and Planetary Science Letters, v. 183, no. 1–2, p. 231–244, https://doi.org/10.1016/S0012-821X(00)00287-9.

Akinin, V., Sobolev, A., Ntaflos, T., and Richter, W., 2005, Clinopyroxene megacrysts from Enmelen melanephelinitic volcanoes (Chukchi Peninsula, Russia): Application to composition and evolution of mantle melts: Contributions to Mineralogy and Petrology, v. 150, no. 1, p. 85–101, https://doi.org/10.1007/s00410-005-0007-x.

Aldiss, D.T., 1981, Plagiogranites from the ocean crust and ophiolites: Nature, v. 289, no. 5798, p. 577–578, https://doi.org/10.1038/289577a0.

Allégre, C.J., Courtillot, V., Tapponnier, P., Hirn, A., Mattauer, M., Coulon, C., Jaeger, J.J., Achache, J., Schärer, U., Marcoux, J., Burg, J.P., Girardeau, J., Armijo, R., Gariépy, C., Göpel, C., Li, T.D., Xiao, X.C., Chang, C.F., Li, G.Q., Lin, B.Y., Teng, J.W., Wang, N.W., Chen, G.M., Han, T.L., Wang, X.B., Den, W.M., Sheng, H.B., Cao, Y.G., Zhou, J., Qiu, H.R., Bao, P.S., Wang, S.C., Wang, B.X., Zhou, Y.X., and Xu, R.H., 1984, Structure and evolution of the Himalaya–Tibet orogenic belt: Nature, v. 307, p. 17–22, https://doi.org/10.1038/307017a0.

An, W., Hu, X., Garzanti, E., BouDagher-Fadel, M.K., Wang, J., and Sun, G., 2014, Xigaze forearc basin revisited (south Tibet): Provenance changes and origin of the Xigaze ophiolite: Geological Society of America Bulletin, v. 126, no. 11–12, p. 1595–1613, https://doi.org/10.1130/B31020.1.

Andersen, T., 2002, Correction of common lead in U-Pb analyses that do not report ^{204}Pb: Chemical Geology, v. 192, no. 1–2, p. 59–79, https://doi.org/10.1016/S0009-2541(02)00195-X.

Arculus, R.J., Ishizuka, O., Bogus, K.A., Gurnis, M., Hickey-Vargas, R., Aljahdali, M.H., Bandini-Maeder, A.N., Barth, A.P., Brandl, P.A., Drab, L., do Monte Guerra, R., Hamada, M., Jiang, F., Kanayama, K., Kender, S., Kusano, Y., Li, H., Loudin, L.C., Maffione, M., Marsaglia, K.M., McCarthy, A., Meffre, S., Morris, A., Neuhaus, M., Savov, I.P., Sena, C., Tepley, F.J., III, van der Land, C., Yogodzinski, G.M., and Zhang, Z., 2015, A record of spontaneous subduction initiation in the Izu-Bonin-Mariana arc: Nature Geoscience, v. 8, p. 728, https://doi.org/10.1038/ngeo2515.

Bao, P.S., Su, L., Wang, J., and Zhai, Q.G., 2013, Study on the tectonic setting for the ophiolites in Xigaze, Tibet: Acta Geologica Sinica–English Edition, v. 87, no. 2, p. 395–425, https://doi.org/10.1111/1755-6724.12058.

Beard, J.S., and Scott, S.R., 2018, A model for the high-temperature origin and paradoxical distribution of pegmatites in mafic plutons, Smartville Complex, California: Journal of Petrology, v. 59, no. 1, p. 3–10, https://doi.org/10.1093/petrology/egy015.

Bédard, É., Hébert, R., Guilmette, C., Lesage, G., Wang, C.S., and Dostal, J., 2009, Petrology and geochemistry of the Saga and Sangsang ophiolitic massifs, Yarlung Zangbo suture zone, southern Tibet: Evidence for an arc–back-arc origin: Lithos, v. 113, no. 1–2, p. 48–67, https://doi.org/10.1016/j.lithos.2009.01.011.

Blichert-Toft, J., and Albarède, F., 1997, The Lu-Hf isotope geochemistry of chondrites and the evolution of the mantle-crust system: Earth and Planetary Science Letters, v. 148, no. 1, p. 243–258, https://doi.org/10.1016/S0012-821X(97)00040-X.

Borghini, G., Rampone, E., Zanetti, A., Class, C., Cipriani, A., Hofmann, A.W., and Goldstein, S.L., 2016, Pyroxenite layers in the Northern Apennines' upper mantle (Italy)—Generation by pyroxenite melting and melt infiltration: Journal of Petrology, v. 57, no. 4, p. 625–653, https://doi.org/10.1093/petrology/egv074.

Brophy, J.G., 2008, A study of rare earth element (REE)–SiO_2 variations in felsic liquids generated by basalt fractionation and amphibolite melting: A potential test for discriminating between the two different processes: Contributions to Mineralogy and Petrology, v. 156, no. 3, p. 337–357, https://doi.org/10.1007/s00410-008-0289-x.

Burg, J.-P., Leyreloup, A., Girardeau, J., and Chen, G.-M., 1987, Structure and metamorphism of a tectonically thickened continental crust: The Yalu Tsangpo suture zone (Tibet): Philosophical Transactions of the Royal Society of London, ser. A, Mathematical and Physical Sciences, v. 321, no. 1557, p. 67–86, https://doi.org/10.1098/rsta.1987.0005.

Carrapa, B., Orme, D.A., DeCelles, P.G., Kapp, P., Cosca, M.A., and Waldrip, R., 2014, Miocene burial and exhumation of the India-Asia collision zone in southern Tibet: Response to slab dynamics and erosion: Geology, v. 42, no. 5, p. 443–446, https://doi.org/10.1130/G35350.1.

Chan, G.H.N., Aitchison, J.C., Crowley, Q.G., Horstwood, M.S.A., Searle, M.P., Parrish, R.R., and Chan, J.S.-L., 2015, U–Pb zircon ages for Yarlung Tsangpo suture zone ophiolites, southwestern Tibet and their tectonic implications: Gondwana Research, v. 27, no. 2, p. 719–732, https://doi.org/10.1016/j.gr.2013.06.016.

Chauvel, C., Marini, J.-C., Plank, T., and Ludden, J.N., 2009, Hf-Nd input flux in the Izu-Mariana subduction zone and recycling of subducted material in the mantle: Geochemistry Geophysics Geosystems, v. 10, no. 1, Q01001, https://doi.org/10.1029/2008GC002101.

Chen, G.W., and Xia, B., 2008, Platinum-group elemental geochemistry of mafic and ultramafic rocks from the Xigaze ophiolite, southern Tibet: Journal of Asian

Earth Sciences, v. 32, no. 5–6, p. 406–422, https://doi.org/10.1016/j.jseaes.2007.11.009.
Chen, G.W., Xia, B., Zhong, Z.H., Wang, G.Q., Wang, H., Zhao, T.P., Wang, J.C., Zhang, L., Qi, L., and Li, S.R., 2003, Geochemical characteristics and geological significance of boninites in the Deji ophiolite, Tibet: Acta Mineralogica Sinica, v. 23, no. 1, p. 91–96.
Chu, M.F., Chung, S.L., Song, B., Liu, D., O'Reilly, S.Y., and Pearson, N.J., 2006, Zircon U-Pb and Hf isotope constraints on the Mesozoic tectonics and crustal evolution of southern Tibet: Geology, v. 34, no. 9, p. 745–748, https://doi.org/10.1130/G22725.1.
Chu, M.F., Chung, S.-L., O'Reilly, S.Y., Pearson, N.J., Wu, F.-Y., Li, X.-H., Liu, D., Ji, J., Chu, C.-H., and Lee, H.-Y., 2011, India's hidden inputs to Tibetan orogeny revealed by Hf isotopes of Transhimalayan zircons and host rocks: Earth and Planetary Science Letters, v. 307, no. 3–4, p. 479–486, https://doi.org/10.1016/j.epsl.2011.05.020.
Coleman, R.G., and Peterman, Z.E., 1975, Oceanic plagiogranite: Journal of Geophysical Research, v. 80, no. 8, p. 1099–1108, https://doi.org/10.1029/JB080i008p01099.
Coltorti, M., Bonadiman, C., Faccini, B., Grégoire, M., O'Reilly, S.Y., and Powell, W., 2007, Amphiboles from suprasubduction and intraplate lithospheric mantle: Lithos, v. 99, no. 1–2, p. 68–84, https://doi.org/10.1016/j.lithos.2007.05.009.
Coogan, L.A., 2003, Contaminating the lower crust in the Oman ophiolite: Geology, v. 31, no. 12, p. 1065–1068, https://doi.org/10.1130/G20129.1.
Coogan, L.A., Wilson, R.N., Gillis, K.M., and MacLeod, C.J., 2001, Near-solidus evolution of oceanic gabbros: Insights from amphibole geochemistry: Geochimica et Cosmochimica Acta, v. 65, no. 23, p. 4339–4357, https://doi.org/10.1016/S0016-7037(01)00714-1.
Coogan, L.A., Gillis, K.M., MacLeod, C.J., Thompson, G.M., and Hékinian, R., 2002, Petrology and geochemistry of the lower ocean crust formed at the East Pacific Rise and exposed at Hess Deep: A synthesis and new results: Geochemistry Geophysics Geosystems, v. 3, no. 11, 8604, https://doi.org/10.1029/2001GC000230.
Cox, J., Searle, M., and Pedersen, R., 1999, The petrogenesis of leucogranitic dykes intruding the northern Semail ophiolite, United Arab Emirates: Field relationships, geochemistry and Sr/Nd isotope systematics: Contributions to Mineralogy and Petrology, v. 137, no. 3, p. 267–287, https://doi.org/10.1007/s004100050550.
Dai, J., Wang, C., Polat, A., Santosh, M., Li, Y., and Ge, Y., 2013, Rapid forearc spreading between 130 and 120 Ma: Evidence from geochronology and geochemistry of the Xigaze ophiolite, southern Tibet: Lithos, v. 172–173, p. 1–16, https://doi.org/10.1016/j.lithos.2013.03.011.
Dai, J.G., Wang, C.S., Zhu, D.C., Li, Y.L., Zhong, H.T., and Ge, Y.K., 2015, Multi-stage volcanic activities and geodynamic evolution of the Lhasa terrane during the Cretaceous: Insights from the Xigaze forearc basin: Lithos, v. 218, p. 127–140, https://doi.org/10.1016/j.lithos.2015.01.019.
Dai, J.G., Wang, C.S., Liu, S.A., Qian, X.Y., Zhu, D.C., and Ke, S., 2016, Deep carbon cycle recorded by calcium-silicate rocks (rodingites) in a subduction-related ophiolite: Geophysical Research Letters, v. 43, no. 22, p. 11635–11643, https://doi.org/10.1002/2016GL070474.
Dilek, Y., and Thy, P., 2006, Age and petrogenesis of plagiogranite intrusions in the Ankara mélange, central Turkey: The Island Arc, v. 15, no. 1, p. 44–57, https://doi.org/10.1111/j.1440-1738.2006.00522.x.
Dilek, Y., Thy, P., Hacker, B., and Grundvig, S., 1999, Structure and petrology of Tauride ophiolites and mafic dike intrusions (Turkey): Implications for the Neotethyan Ocean: Geological Society of America Bulletin, v. 111, no. 8, p. 1192–1216, https://doi.org/10.1130/0016-7606(1999)111<1192:SAPOTO>2.3.CO;2.
Dilek, Y., Furnes, H., and Shallo, M., 2008, Geochemistry of the Jurassic Mirdita ophiolite (Albania) and the MORB to SSZ evolution of a marginal basin oceanic crust: Lithos, v. 100, no. 1–4, p. 174–209, https://doi.org/10.1016/j.lithos.2007.06.026.
Dixon, S., and Rutherford, M.J., 1979, Plagiogranites as late-stage immiscible liquids in ophiolite and mid-ocean ridge suites: An experimental study: Earth and Planetary Science Letters, v. 45, no. 1, p. 45–60, https://doi.org/10.1016/0012-821X(79)90106-7.
Dubois-Côté, V., Hébert, R., Dupuis, C., Wang, C.S., Li, Y.L., and Dostal, J., 2005, Petrological and geochemical evidence for the origin of the Yarlung Zangbo ophiolites, southern Tibet: Chemical Geology, v. 214, no. 3–4, p. 265–286, https://doi.org/10.1016/j.chemgeo.2004.10.004.
Dürr, S.B., 1996, Provenance of Xigaze fore-arc basin clastic rocks (Cretaceous, south Tibet): Geological Society of America Bulletin, v. 108, no. 6, p. 669–684, https://doi.org/10.1130/0016-7606(1996)108<0669:POXFAB>2.3.CO;2.
Ewart, A., and Hawkesworth, C.J., 1987, The Pleistocene–Recent Tonga-Kermadec arc lavas: Interpretation of new isotopic and rare earth data in terms of a depleted mantle source model: Journal of Petrology, v. 28, no. 3, p. 495–530, https://doi.org/10.1093/petrology/28.3.495.
Gaetani, G., Kent, A.R., Grove, T., Hutcheon, I., and Stolper, E., 2003, Mineral/melt partitioning of trace elements during hydrous peridotite partial melting: Contributions to Mineralogy and Petrology, v. 145, no. 4, p. 391–405, https://doi.org/10.1007/s00410-003-0447-0.
Gale, A., Dalton, C.A., Langmuir, C.H., Su, Y., and Schilling, J.-G., 2013, The mean composition of ocean ridge basalts: Geochemistry Geophysics Geosystems, v. 14, no. 3, p. 489–518, https://doi.org/10.1029/2012GC004334.
Gao, J.F., Lu, J.J., Lai, M.Y., Lin, Y.P., and Pu, W., 2003, Analysis of trace elements in rock samples using HR-ICPMS: Journal of Nanjing University [Natural Sciences], v. 39, p. 844–850.
Gao, S., Liu, X., Yuan, H., Hattendorf, B., Günther, D., Chen, L., and Hu, S., 2002, Determination of forty-two major and trace elements in USGS and NIST SRM glasses by laser ablation–inductively coupled plasma–mass spectrometry: Geostandards Newsletter, v. 26, no. 2, p. 181–196, https://doi.org/10.1111/j.1751-908X.2002.tb00886.x.
Gibbons, A.D., Zahirovic, S., Müller, R.D., Whittaker, J.M., and Yatheesh, V., 2015, A tectonic model reconciling evidence for the collisions between India, Eurasia and intra-oceanic arcs of the central-eastern Tethys: Gondwana Research, v. 28, no. 2, p. 451–492, https://doi.org/10.1016/j.gr.2015.01.001.
Gillis, K., and Coogan, L., 2002, Anatectic migmatites from the roof of an ocean ridge magma chamber: Journal of Petrology, v. 43, no. 11, p. 2075–2095, https://doi.org/10.1093/petrology/43.11.2075.
Girardeau, J., Mercier, J.C.C., and Xibin, W., 1985a, Petrology of the mafic rocks of the Xigaze ophiolite, Tibet: Implications for the genesis of the oceanic lithosphere: Contributions to Mineralogy and Petrology, v. 90, no. 4, p. 309–321, https://doi.org/10.1007/BF00384710.
Girardeau, J., Mercier, J.C.C., and Yougong, Z., 1985b, Origin of the Xigaze ophiolite, Yarlung Zangbo suture zone, southern Tibet: Tectonophysics, v. 119, no. 1–4, p. 407–433, https://doi.org/10.1016/0040-1951(85)90048-4.
Godard, M., Dautria, J.-M., and Perrin, M., 2003, Geochemical variability of the Oman ophiolite lavas: Relationship with spatial distribution and paleomagnetic directions: Geochemistry Geophysics Geosystems, v. 4, no. 6, 8609, https://doi.org/10.1029/2002GC000452.
Goodenough, K.M., Thomas, R.J., Styles, M.T., Schofield, D.I., and MacLeod, C.J., 2014, Records of ocean growth and destruction in the Oman–UAE ophiolite: Elements, v. 10, no. 2, p. 109–114, https://doi.org/10.2113/gselements.10.2.109.
Griffin, W.L., Pearson, N.J., Belousova, E., Jackson, S.E., van Achterbergh, E., O'Reilly, S.Y., and Shee, S.R., 2000, The Hf isotope composition of cratonic mantle: LAM-MC-ICPMS analysis of zircon megacrysts in kimberlites: Geochimica et Cosmochimica Acta, v. 64, no. 1, p. 133–147, https://doi.org/10.1016/S0016-7037(99)00343-9.
Griffin, W.L., Afonso, J.C., Belousova, E.A., Gain, S.E., Gong, X.H., González-Jiménez, J.M., Howell, D., Huang, J.X., McGowan, N., Pearson, N.J., Satsukawa, T., Shi, R., Williams, P., Xiong, Q., Yang, J.S., Zhang, M., and O'Reilly, S.Y., 2016, Mantle recycling: Transition zone metamorphism of Tibetan ophiolitic peridotites and its tectonic implications: Journal of Petrology, v. 57, no. 4, p. 655–684, https://doi.org/10.1093/petrology/egw011.
Guan, Q., Zhu, D.C., Zhao, Z.D., Dong, G.C., Zhang, L.L., Li, X.W., Liu, M., Mo, X.X., Liu, Y.S., and Yuan, H.L., 2012, Crustal thickening prior to 38 Ma in southern Tibet: Evidence from lower crust–derived adakitic magmatism in the Gangdese Batholith: Gondwana Research, v. 21, no. 1, p. 88–99, https://doi.org/10.1016/j.gr.2011.07.004.
Guilmette, C., Hébert, R., Wang, C., and Villeneuve, M., 2009, Geochemistry and geochronology of the metamorphic sole underlying the Xigaze ophiolite, Yarlung Zangbo suture zone, south Tibet: Lithos, v. 112, no. 1–2, p. 149–162, https://doi.org/10.1016/j.lithos.2009.05.027.
Guilmette, C., Hebert, R., Dostal, J., Indares, A., Ullrich, T., Bedard, E., and Wang, C.S., 2012, Discovery of a dismembered metamorphic sole in the Saga ophiolitic melange, South Tibet: Assessing an Early Cretaceous disruption of the Neo-Tethyan supra-subduction zone and consequences on basin closing: Gondwana Research, v. 22, no. 2, p. 398–414, https://doi.org/10.1016/j.gr.2011.10.012.
Guo, L., Zhang, H.-F., Harris, N., Pan, F.-B., and Xu, W.-C., 2013, Late Cretaceous (~81 Ma) high-temperature metamorphism in the southeastern Lhasa terrane: Implication for the Neo-Tethys ocean ridge subduction: Tectonophysics, v. 608, p. 112–126, https://doi.org/10.1016/j.tecto.2013.10.007.
Hampel, A., Kukowski, N., Bialas, J., Huebscher, C., and Heinbockel, R., 2004, Ridge subduction at an erosive margin: The collision zone of the Nazca Ridge in southern Peru: Journal of Geophysical Research–Solid Earth, v. 109, no. B2, B02101, https://doi.org/10.1029/2003jb002593.
Harlov, D.E., Van Den Kerkhof, A., and Johansson, L., 2014, High-grade localized metasomatic alteration of the granitic gneiss surrounding a clinopyroxene-rich pegmatoid dyke: Söndrum Stenhuggeriet, Halmstad, SW Sweden: Journal of Metamorphic Geology, v. 32, no. 4, p. 389–416, https://doi.org/10.1111/jmg.12077.
Hébert, R., Huot, F., Wang, C.S., and Liu, Z.F., 2003, Yarlung Zangbo ophiolites (southern Tibet) revisited: Geodynamic implications from the mineral record, *in* Dilek, Y., and Robinson, P.T., eds., Ophiolites in Earth History: Geological Society [London] Special Publication 218, p. 165–190, https://doi.org/10.1144/GSL.SP.2003.218.01.10.
Hébert, R., Bezard, R., Guilmette, C., Dostal, J., Wang, C.S., and Liu, Z.F., 2012, The Indus–Yarlung Zangbo ophiolites from Nanga Parbat to Namche Barwa syntaxes, southern Tibet: First synthesis of petrology, geochemistry, and geochronology with incidences on geodynamic reconstructions of Neo-Tethys: Gondwana Research, v. 22, no. 2, p. 377–397, https://doi.org/10.1016/j.gr.2011.10.013.
Hickey-Vargas, R., Yogodzinski, G.M., Ishizuka, O., McCarthy, A., Bizimis, M., Kusano, Y., Savov, I.P., and Arculus, R., 2018, Origin of depleted basalts during subduction initiation and early development of the Izu-Bonin-Mariana island arc: Evidence from IODP expedition 351 Site U1438, Amami-Sankaku basin: Geochimica et Cosmochimica Acta, v. 229, p. 85–111, https://doi.org/10.1016/j.gca.2018.03.007.
Hofmann, A.W., 1997, Mantle geochemistry: The message from oceanic volcanism: Nature, v. 385, p. 219–229, https://doi.org/10.1038/385219a0.
Hu, H., and Stern, R.J., 2020, Early Cretaceous subduction initiation beneath southern Tibet caused the northward flight of India: Geoscience Frontiers, v. 11, no. 4, p. 1123–1131, https://doi.org/10.1016/j.gsf.2020.01.010.
Huang, F., Xu, J.-F., Chen, J.-L., Wu, J.-B., Zeng, Y.-C., Xiong, Q.-W., Chen, X.-F., and Yu, H.-X., 2016, Two Cenozoic tectonic events of N-S and E-W extension in the Lhasa terrane: Evidence from geology and geochronology: Lithos, v. 245, p. 118–132, https://doi.org/10.1016/j.lithos.2015.08.014.

Huang, W., van Hinsbergen, D.J.J., Maffione, M., Orme, D.A., Dupont-Nivet, G., Guilmette, C., Ding, L., Guo, Z., and Kapp, P., 2015, Lower Cretaceous Xigaze ophiolites formed in the Gangdese forearc: Evidence from paleomagnetism, sediment provenance, and stratigraphy: Earth and Planetary Science Letters, v. 415, p. 142–153, https://doi.org/10.1016/j.epsl.2015.01.032.

Ishizuka, O., Tani, K., Reagan, M.K., Kanayama, K., Umino, S., Harigane, Y., Sakamoto, I., Miyajima, Y., Yuasa, M., and Dunkley, D.J., 2011, The timescales of subduction initiation and subsequent evolution of an oceanic island arc: Earth and Planetary Science Letters, v. 306, no. 3–4, p. 229–240, https://doi.org/10.1016/j.epsl.2011.04.006.

Ishizuka, O., Tani, K., and Reagan, M.K., 2014, Izu-Bonin-Mariana Forearc Crust as a Modern Ophiolite Analogue: Elements, v. 10, no. 2, p. 115–120, https://doi.org/10.2113/gselements.10.2.115.

Ishizuka, O., Hickey-Vargas, R., Arculus, R.J., Yogodzinski, G.M., Savov, I.P., Kusano, Y., McCarthy, A., Brandl, P.A., and Sudo, M., 2018, Age of Izu-Bonin-Mariana arc basement: Earth and Planetary Science Letters, v. 481, p. 80–90, https://doi.org/10.1016/j.epsl.2017.10.023.

Jackson, S.E., Pearson, N.J., Griffin, W.L., and Belousova, E.A., 2004, The application of laser ablation–inductively coupled plasma–mass spectrometry to in situ U-Pb zircon geochronology: Chemical Geology, v. 211, no. 1–2, p. 47–69, https://doi.org/10.1016/j.chemgeo.2004.06.017.

Ji, W.-Q., Wu, F.-Y., Chung, S.-L., Li, J.-X., and Liu, C.-Z., 2009, Zircon U-Pb geochronology and Hf isotopic constraints on petrogenesis of the Gangdese batholith, southern Tibet: Chemical Geology, v. 262, no. 3–4, p. 229–245, https://doi.org/10.1016/j.chemgeo.2009.01.020.

Ji, W.Q., Wu, F.Y., Liu, C.Z., and Chung, S.L., 2012, Early Eocene crustal thickening in southern Tibet: New age and geochemical constraints from the Gangdese Batholith: Journal of Asian Earth Sciences, v. 53, p. 82–95, https://doi.org/10.1016/j.jseaes.2011.08.020.

Kaczmarek, M.-A., Jonda, L., and Davies, H., 2015, Evidence of melting, melt percolation and deformation in a supra-subduction zone (Marum ophiolite complex, Papua New Guinea): Contributions to Mineralogy and Petrology, v. 170, no. 2, p. 1–23, https://doi.org/10.1007/s00410-015-1174-z.

Kang, Z.-Q., Xu, J.-F., Wilde, S.A., Feng, Z.-H., Chen, J.-L., Wang, B.-D., Fu, W.-C., and Pan, H.-B., 2014, Geochronology and geochemistry of the Sangri Group volcanic rocks, southern Lhasa terrane: Implications for the early subduction history of the Neo-Tethys and Gangdese magmatic arc: Lithos, v. 200–201, p. 157–168, https://doi.org/10.1016/j.lithos.2014.04.019.

Kapp, P., and DeCelles, P.G., 2019, Mesozoic–Cenozoic geological evolution of the Himalayan-Tibetan orogen and working tectonic hypotheses: American Journal of Science, v. 319, no. 3, p. 159–254, https://doi.org/10.2475/03.2019.01.

Kapp, P., DeCelles, P., Gehrels, G., Heizler, M., and Ding, L., 2007, Geological records of the Lhasa-Qiangtang and Indo-Asian collisions in the Nima area of central Tibet: Geological Society of America Bulletin, v. 119, no. 7–8, p. 917–932, https://doi.org/10.1130/B26033.1.

Kobayashi, K., and Nakamura, E., 2001, Geochemical evolution of Akagi Volcano, NE Japan: Implications for interaction between island-arc magma and lower crust, and generation of isotopically various magmas: Journal of Petrology, v. 42, no. 12, p. 2303–2331, https://doi.org/10.1093/petrology/42.12.2303.

Koepke, J., Feig, S., Snow, J., and Freise, M., 2004, Petrogenesis of oceanic plagiogranites by partial melting of gabbros: An experimental study: Contributions to Mineralogy and Petrology, v. 146, no. 4, p. 414–432, https://doi.org/10.1007/s00410-003-0511-9.

Koepke, J., Berndt, J., Feig, S., and Holtz, F., 2007, The formation of SiO_2-rich melts within the deep oceanic crust by hydrous partial melting of gabbros: Contributions to Mineralogy and Petrology, v. 153, no. 1, p. 67–84, https://doi.org/10.1007/s00410-006-0135-y.

Koepke, J., Schoenborn, S., Oelze, M., Wittmann, H., Feig, S.T., Hellebrand, E., Boudier, F., and Schoenberg, R., 2009, Petrogenesis of crustal wehrlites in the Oman ophiolite: Experiments and natural rocks: Geochemistry Geophysics Geosystems, v. 10, no. 10, Q10002, https://doi.org/10.1029/2009GC002488.

Leake, B.E., Woolley, A.R., Kisch, H.J., Krivovichev, V.G., Linthout, K., Laird, J., Maresch, W.V., Schumacher, J.C., Stephenson, N.C., and Whittaker, E.J., 1997, Nomenclature of amphiboles: Report of the Subcommittee on Amphiboles of the International Mineralogical Association, Commission on New Minerals and Mineral Names: Canadian Mineralogist, v. 35, p. 219–246.

Li, J.F., Xia, B., Liu, L.W., Xu, L.F., He, G.S., Wang, H., Zhang, Y.Q., and Yang, Z.Q., 2009, SHRIMP U-Pb dating for the gabbro in the Qunrang ophiolite, Tibet: The geochronology constraint for the development of eastern Tethys basin: Geotectonica et Metallogenia, v. 33, no. 2, p. 294–298.

Li, W.X., Zhao, Z.D., Zhu, D.C., Dung, G.C., Zhou, S., Mo, X.X., DePaolo, D., and Dilek, Y., 2012, Geochemical discrimination of tectonic environments of the Yarlung Zangpo ophiolite in southern Tibet: Acta Petrologica Sinica (Yanshi Xuebao), v. 28, no. 5, p. 1663–1673.

Liu, C.-Z., Zhang, C., Yang, L.-Y., Zhang, L.-L., Ji, W.-Q., and Wu, F.-Y., 2014, Formation of gabbronorites in the Purang ophiolite (SW Tibet) through melting of hydrothermally altered mantle along a detachment fault: Lithos, v. 205, p. 127–141, https://doi.org/10.1016/j.lithos.2014.06.019.

Liu, T., Wu, F.-Y., Zhang, L.-L., Zhai, Q.-G., Liu, C.-Z., Ji, W.-B., Zhang, C., and Xu, Y., 2016, Zircon U-Pb geochronological constraints on rapid exhumation of the mantle peridotite of the Xigaze ophiolite, southern Tibet: Chemical Geology, v. 443, p. 67–86, https://doi.org/10.1016/j.chemgeo.2016.09.015.

Liu, T., Wu, F.-Y., Liu, C.-Z., Tribuzio, R., Ji, W.-B., Zhang, C., Xu, Y., and Zhang, W.-Q., 2018, Variably evolved gabbroic intrusions within the Xigaze ophiolite (Tibet): New insights into the origin of ophiolite diversity: Contributions to Mineralogy and Petrology, v. 173, no. 11, p. 91, https://doi.org/10.1007/s00410-018-1518-6.

Liu, T., Wu, F.-Y., Liu, C.-Z., Zhang, C., Ji, W.-B., and Xu, Y., 2019, Reconsideration of Neo-Tethys evolution constrained from the nature of the Dazhuqu ophiolitic mantle, southern Tibet: Contributions to Mineralogy and Petrology, v. 174, no. 3, p. 23, https://doi.org/10.1007/s00410-019-1557-7.

Ludwig, K.R., 2008, User's Manual for Isoplot 3.60: Berkeley Geochronology Center Special Publication 4, 77 p.

Ma, L., Wang, Q., Wyman, D.A., Li, Z.-X., Jiang, Z.-Q., Yang, J.-H., Gou, G.-N., and Guo, H.-F., 2013, Late Cretaceous (100–89 Ma) magnesian charnockites with adakitic affinities in the Milin area, eastern Gangdese: Partial melting of subducted oceanic crust and implications for crustal growth in southern Tibet: Lithos, v. 175–176, p. 315–332, https://doi.org/10.1016/j.lithos.2013.04.006.

MacLeod, C.J., Johan Lissenberg, C., and Bibby, L.E., 2013, "Moist MORB" axial magmatism in the Oman ophiolite: The evidence against a mid-ocean ridge origin: Geology, v. 41, no. 4, p. 459–462, https://doi.org/10.1130/G33904.1.

Maffione, M., van Hinsbergen, D.J.J., Koornneef, L.M.T., Guilmette, C., Hodges, K., Borneman, N., Huang, W., Ding, L., and Kapp, P., 2015, Forearc hyperextension dismembered the south Tibetan ophiolites: Geology, v. 43, no. 6, p. 475–478, https://doi.org/10.1130/G36472.1.

Malpas, J., Zhou, M.F., Robinson, P.T., and Reynolds, P.H., 2003, Geochemical and geochronological constraints on the origin and emplacement of the Yarlung Zangbo ophiolites, southern Tibet, *in* Dilek, Y., and Robinson, P.T., eds., Ophiolites in Earth History: Geological Society [London] Special Publication 218, p. 191–206, https://doi.org/10.1144/GSL.SP.2003.218.01.11.

McDermid, I.R.C., Aitchison, J.C., Davis, A.M., Harrison, T.M., and Grove, M., 2002, The Zedong terrane: a Late Jurassic intra-oceanic magmatic arc within the Yarlung-Tsangpo suture zone, southeastern: Chemical Geology, v. 187, no. 3, p. 267–277, https://doi.org/10.1016/S0009-2541(02)00040-2.

McDonough, W., and Sun, S., 1995, The composition of the Earth: Chemical Geology, v. 120, no. 3–4, p. 223–253, https://doi.org/10.1016/0009-2541(94)00140-4.

Meffre, S., Falloon, T.J., Crawford, T.J., Hoernle, K., Hauff, F., Duncan, R.A., Bloomer, S.H., and Wright, D.J., 2012, Basalts erupted along the Tongan fore arc during subduction initiation: Evidence from geochronology of dredged rocks from the Tonga fore arc and trench: Geochemistry Geophysics Geosystems, v. 13, no. 12, Q12003, https://doi.org/10.1029/2012GC004335.

Metcalf, K., and Kapp, P., 2019, History of subduction erosion and accretion recorded in the Yarlung suture zone, southern Tibet, *in* Treloar, P.J., and Searle, M.P., eds., Himalayan Tectonics: Geological Society [London] Special Publication 483, p. 517–554, https://doi.org/10.1144/SP483.12.

Moores, E.M., Kellogg, L.H., and Dilek, Y., 2000, Tethyan ophiolites, mantle convection, and tectonic "historical contingency": A resolution of the "ophiolite conundrum," *in* Dilek, Y., et al., eds., Ophiolites and Oceanic Crust: New Insights from Field Studies and Ocean Drilling Program: Geological Society of America Special Paper 349, p. 3–12, https://doi.org/10.1130/0-8137-2349-3.3.

Nicolas, A., Girardeau, J., Marcoux, J., Dupre, B., Wang, X.B., Cao, Y.G., Zheng, H.X., and Xiao, X.C., 1981, The Xigaze ophiolite (Tibet): A peculiar oceanic lithosphere: Nature, v. 294, p. 414–417, https://doi.org/10.1038/294414a0.

Niu, X.L., Zhao, Z.D., Mo, X.X., Depaolo, D.J., Dong, G., Zhang, S.Q., Zhu, D.C., and Guo, T.Y., 2006, Elemental and Sr-Nd-Pb isotopic geochemistry for basic rocks from Decun-Angren ophiolites in Xigaze area, Tibet: Implications for the characteristics of the Tethyan upper mantle domain: Acta Petrologica Sinica (Yanshi Xuebao), v. 22, no. 12, p. 2875–2888.

Pan, F.-B., Zhang, H.-F., Xu, W.-C., Guo, L., Luo, B.-J., and Wang, S., 2016, U-Pb zircon dating, geochemical and Sr-Nd-Hf isotopic compositions of Motuo quartz–monzonite: Implication for the genesis and diversity of the high Ba-Sr granitoids in orogenic belt: Tectonophysics, v. 668–669, p. 52–64, https://doi.org/10.1016/j.tecto.2015.12.007.

Parlak, O., 2016, The Tauride ophiolites of Anatolia (Turkey): A review: Journal of Earth Science, v. 27, no. 6, p. 901–934, https://doi.org/10.1007/s12583-016-0679-3.

Parlak, O., Dunkl, I., Karaoğlan, F., Kusky, T.M., Zhang, C., Wang, L., Koepke, J., Billor, Z., Hames, W.E., Şimşek, E., Şimşek, G., Şimşek, T., and Öztürk, S.E., 2019, Rapid cooling history of a Neotethyan ophiolite: Evidence for contemporaneous subduction initiation and metamorphic sole formation: Geological Society of America Bulletin, v. 131, no. 11–12, p. 2011–2038, https://doi.org/10.1130/B35040.1.

Pearce, J.A., Harris, N.B.W., and Tindle, A.G., 1984, Trace element discrimination diagrams for the tectonic interpretation of granitic rocks: Journal of Petrology, v. 25, no. 4, p. 956–983, https://doi.org/10.1093/petrology/25.4.956.

Pearce, J.A., Barker, P.E., Harvey, P.K., and Luff, I.W., 1995, Geochemical evidence for subduction fluxes, mantle melting and fractional crystallization beneath the South Sandwich island arc: Journal of Petrology, v. 36, no. 4, p. 1073–1109, https://doi.org/10.1093/petrology/36.4.1073.

Pedersen, R., and Malpas, J., 1984, The origin of oceanic plagiogranites from the Karmoy ophiolite, western Norway: Contributions to Mineralogy and Petrology, v. 88, no. 1–2, p. 36–52, https://doi.org/10.1007/BF00371410.

Piccardo, G. B., Padovano, M., and Guarnieri, L., 2014, The Ligurian Tethys: Mantle processes and geodynamics: Earth-Science Reviews, v. 138, p. 409–434, https://doi.org/10.1016/j.earscirev.2014.07.002.

Putirka, K.D., 2008, Thermometers and barometers for volcanic systems: Reviews in Mineralogy and Geochemistry, v. 69, no. 1, p. 61–120, https://doi.org/10.2138/rmg.2008.69.3.

Python, M., and Ceuleneer, G., 2003, Nature and distribution of dykes and related melt migration structures in the mantle section of the Oman ophiolite: Geochemistry

Geophysics Geosystems, v. 4, no. 7, 8612, https://doi.org/10.1029/2002GC000354.
Reagan, M.K., Ishizuka, O., Stern, R.J., Kelley, K.A., Ohara, Y., Blichert-Toft, J., Bloomer, S.H., Cash, J., Fryer, P., Hanan, B.B., Hickey-Vargas, R., Ishii, T., Kimura, J.-I., Peate, D.W., Rowe, M.C., and Woods, M., 2010, Fore-arc basalts and subduction initiation in the Izu-Bonin-Mariana system: Geochemistry Geophysics Geosystems, v. 11, no. 3, Q03X12, https://doi.org/10.1029/2009GC002871.
Reagan, M.K., McClelland, W.C., Girard, G., Goff, K.R., Peate, D.W., Ohara, Y., and Stern, R.J., 2013, The geology of the southern Mariana fore-arc crust: Implications for the scale of Eocene volcanism in the western Pacific: Earth and Planetary Science Letters, v. 380, p. 41–51, https://doi.org/10.1016/j.epsl.2013.08.013.
Reagan, M.K., Pearce, J.A., Petronotis, K., Almeev, R.R., Avery, A.J., Carvallo, C., Chapman, T., Christeson, G.L., Ferré, E.C., Godard, M., Heaton, D.E., Kirchenbaur, M., Kurz, W., Kutterolf, S., Li, H., Li, Y., Michibayashi, K., Morgan, S., Nelson, W.R., Prytulak, J., Python, M., Robertson, A.H.F., Ryan, J.G., Sager, W.W., Sakuyama, T., Shervais, J.W., Shimizu, K., and Whattam, S.A., 2017, Subduction initiation and ophiolite crust: New insights from IODP drilling: International Geology Review, v. 59, no. 11, p. 1439–1450, https://doi.org/10.1080/00206814.2016.1276482.
Reagan, M.K., Heaton, D.E., Schmitz, M.D., Pearce, J.A., Shervais, J.W., and Koppers, A.A.P., 2019, Forearc ages reveal extensive short-lived and rapid seafloor spreading following subduction initiation: Earth and Planetary Science Letters, v. 506, p. 520–529, https://doi.org/10.1016/j.epsl.2018.11.020.
Ridolfi, F., Renzulli, A., and Puerini, M., 2010, Stability and chemical equilibrium of amphibole in calc-alkaline magmas: An overview, new thermobarometric formulations and application to subduction-related volcanoes: Contributions to Mineralogy and Petrology, v. 160, no. 1, p. 45–66, https://doi.org/10.1007/s00410-009-0465-7.
Rollinson, H., 2009, New models for the genesis of plagiogranites in the Oman ophiolite: Lithos, v. 112, no. 3–4, p. 603–614, https://doi.org/10.1016/j.lithos.2009.06.006.
Rollinson, H., 2015, Slab and sediment melting during subduction initiation: Granitoid dykes from the mantle section of the Oman ophiolite: Contributions to Mineralogy and Petrology, v. 170, no. 3, p. 1–20, https://doi.org/10.1007/s00410-015-1177-9.
Saccani, E., and Photiades, A., 2004, Mid-ocean ridge and supra-subduction affinities in the Pindos ophiolites (Greece): Implications for magma genesis in a forearc setting: Lithos, v. 73, no. 3–4, p. 229–253, https://doi.org/10.1016/j.lithos.2003.12.002.
Santosh, M., Rajesh, V.J., Tsunogae, T., and Arai, S., 2010, Diopsidites from a Neoproterozoic–Cambrian suture in southern India: Geological Magazine, v. 147, no. 5, p. 777–788, https://doi.org/10.1017/S0016756810000154.
Singh, A.K., Chung, S.-L., Bikramaditya, R.K., and Lee, H.Y., 2017, New U-Pb zircon ages of plagiogranites from the Nagaland–Manipur ophiolites, Indo-Myanmar orogenic belt, NE India: Journal of the Geological Society [London], v. 174, no. 1, p. 170–179, https://doi.org/10.1144/jgs2016-048.
Sobolev, A., Migdisov, A., and Portnyagin, M., 1996, Incompatible element partitioning between clinopyroxene and basalt liquid revealed by the study of melt inclusions in minerals from Troodos lavas, Cyprus: Petrology, v. 4, no. 3, p. 307–317.
Stern, R.J., 2004, Subduction initiation: Spontaneous and induced: Earth and Planetary Science Letters, v. 226, no. 3–4, p. 275–292, https://doi.org/10.1016/S0012-821X(04)00498-4.
Stern, R.J., and Gerya, T., 2018, Subduction initiation in nature and models: A review: Tectonophysics, v. 746, p. 173–198, https://doi.org/10.1016/j.tecto.2017.10.014.
Stern, R.J., Reagan, M., Ishizuka, O., Ohara, Y., and Whattam, S., 2012, To understand subduction initiation, study forearc crust: To understand forearc crust, study ophiolites: Lithosphere, v. 4, no. 6, p. 469–483, https://doi.org/10.1130/L183.1.
Stern, R.J., Gerya, T., and Tackley, P.J., 2018, Stagnant lid tectonics: Perspectives from silicate planets, dwarf planets, large moons, and large asteroids: Geoscience Frontiers, v. 9, no. 1, p. 103–119, https://doi.org/10.1016/j.gsf.2017.06.004.
Sun, S., and McDonough, W., 1989, Chemical and isotopic systematics of oceanic basalts: Implications for mantle composition and processes, *in* Saunders, A.D., and Norry, M.J., eds., Magmatism in the Ocean Basins: Geological Society [London] Special Publication 42, p. 313–345, https://doi.org/10.1144/GSL.SP.1989.042.01.19.
Wang, C., Li, X., Liu, Z., Li, Y., Jansa, L., Dai, J., and Wei, Y., 2012, Revision of the Cretaceous–Paleogene stratigraphic framework, facies architecture and provenance of the Xigaze forearc basin along the Yarlung Zangbo suture zone: Gondwana Research, v. 22, no. 2, p. 415–433, https://doi.org/10.1016/j.gr.2011.09.014.
Wang, J.-G., Hu, X., Garzanti, E., An, W., and Liu, X.-C., 2017, The birth of the Xigaze forearc basin in southern Tibet: Earth and Planetary Science Letters, v. 465, p. 38–47, https://doi.org/10.1016/j.epsl.2017.02.036.
Wang, Q., Zhu, D.C., Cawood, P.A., Zhao, Z.D., Liu, S.A., Chung, S.L., Zhang, L.L., Liu, D., Zheng, Y.C., and Dai, J.G., 2015, Eocene magmatic processes and crustal thickening in southern Tibet: Insights from strongly fractionated ca. 43 Ma granites in the western Gangdese Batholith: Lithos, v. 239, p. 128–141, https://doi.org/10.1016/j.lithos.2015.10.003.
Wang, R., Xia, B., Zhou, G., Zhang, Y., Yang, Z., Li, W., Wei, D., Zhong, L., and Xu, L., 2006, SHRIMP zircon U-Pb dating for gabbro from the Tiding ophiolite in Tibet: Chinese Science Bulletin, v. 51, no. 14, p. 1776–1779, https://doi.org/10.1007/s11434-006-2027-y.
Wang, X.B., Bao, P.S., and Xiao, X.C., 1987, Ophiolites of the Yarlung Zangbo River, Xizang (Tibet): Beijing, Publishing House of Surveying and Mapping, 117 p.
Wang, X.-C., Liu, W.-L., Zhong, Y., Hu, X.-C., Xia, B., and Huang, W., 2018, Geochemical and zircon U-Pb age constraints on the origin of the Mesozoic Xigaze ophiolite, Yarlung Zangbo suture zone, SW China: International Geology Review, v. 60, no. 10, p. 1267–1289 https://doi.org/10.1080/00206814.2017.1385034.
Whattam, S.A., and Stern, R.J., 2011, The 'subduction initiation rule': A key for linking ophiolites, intra-oceanic forearcs, and subduction initiation: Contributions to Mineralogy and Petrology, v. 162, no. 5, p. 1031–1045, https://doi.org/10.1007/s00410-011-0638-z.
Wu, F.-Y., Yang, Y.-H., Xie, L.-W., Yang, J.-H., and Xu, P., 2006, Hf isotopic compositions of the standard zircons and baddeleyites used in U-Pb geochronology: Chemical Geology, v. 234, no. 1–2, p. 105–126, https://doi.org/10.1016/j.chemgeo.2006.05.003.
Wu, F.Y., Ji, W.Q., Liu, C.Z., and Chung, S.L., 2010, Detrital zircon U-Pb and Hf isotopic data from the Xigaze fore-arc basin: Constraints on Transhimalayan magmatic evolution in southern Tibet: Chemical Geology, v. 271, no. 1–2, p. 13–25, https://doi.org/10.1016/j.chemgeo.2009.12.007.
Wu, F.Y., Liu, C.Z., Zhang, L.L., Zhang, C., Wang, J.G., Ji, W.Q., and Liu, X.C., 2014a, Yarlung Zangbo ophiolite: A critical updated view: Acta Petrologica Sinica (Yanshi Xuebao), v. 30, no. 2, p. 293–325.
Wu, F.-Y., Ji, W.-Q., Wang, J.-G., Liu, C.-Z., Chung, S.-L., and Clift, P.D., 2014b, Zircon U-Pb and Hf isotopic constraints on the onset time of India-Asia collision: American Journal of Science, v. 314, no. 2, p. 548–579, https://doi.org/10.2475/02.2014.04.
Xiong, F., Yang, J., Robinson, P.T., Gao, J., Chen, Y., and Lai, S., 2017, Petrology and geochemistry of peridotites and podiform chromitite in the Xigaze ophiolite, Tibet: Implications for a suprasubduction zone origin: Journal of Asian Earth Sciences, v. 146, supplement C, p. 56–75, https://doi.org/10.1016/j.jseaes.2017.05.001.
Xiong, Q., Griffin, W.L., Zheng, J.-P., O'Reilly, S.Y., Pearson, N.J., Xu, B., and Belousova, E.A., 2016, Southward trench migration at ~130–120 Ma caused accretion of the Neo-Tethyan forearc lithosphere in Tibetan ophiolites: Earth and Planetary Science Letters, v. 438, p. 57–65, https://doi.org/10.1016/j.epsl.2016.01.014.
Xu, B., Hou, Z.-Q., Zheng, Y.-C., Wang, R., He, M.-Y., Zhou, L.-M., Wang, Z.-X., He, W.-Y., Zhou, Y., and Yang, Y., 2017, In situ elemental and isotopic study of diorite intrusions: Implication for Jurassic arc magmatism and porphyry Cu-Au mineralisation in southern Tibet: Ore Geology Reviews, v. 90, p. 1063–1077, https://doi.org/10.1016/j.oregeorev.2017.04.036.
Xu, W.-C., Zhang, H.-F., Luo, B.-j., Guo, L., and Yang, H., 2015, Adakite-like geochemical signature produced by amphibole-dominated fractionation of arc magmas: An example from the Late Cretaceous magmatism in Gangdese belt, south Tibet: Lithos, v. 232, p. 197–210, https://doi.org/10.1016/j.lithos.2015.07.001.
Xu, Y., Liu, J., Xiong, Q., Su, B.-X., Scott, J.M., Xu, B., Zhu, D.-C., and Pearson, D.G., 2020, The complex life cycle of oceanic lithosphere: A study of Yarlung-Zangbo ophiolitic peridotites, Tibet: Geochimica et Cosmochimica Acta, v. 277, p. 175–191, https://doi.org/10.1016/j.gca.2020.03.024.
Yamasaki, T., Maeda, J., and Mizuta, T., 2006, Geochemical evidence in clinopyroxenes from gabbroic sequence for two distinct magmatisms in the Oman ophiolite: Earth and Planetary Science Letters, v. 251, no. 1–2, p. 52–65, https://doi.org/10.1016/j.epsl.2006.08.027.
Yang, J.-S., Robinson, P.T., and Dilek, Y., 2014, Diamonds in Ophiolites: Elements, v. 10, no. 2, p. 127–130, https://doi.org/10.2113/gselements.10.2.127.
Yang, Z., Hou, Z., Chang, Z., Li, Q., Liu, Y., Qu, H., Sun, M., and Xu, B., 2016, Cospatial Eocene and Miocene granitoids from the Jiru Cu deposit in Tibet: Petrogenesis and implications for the formation of collisional and postcollisional porphyry Cu systems in continental collision zones: Lithos, v. 245, p. 243–257, https://doi.org/10.1016/j.lithos.2015.04.002.
Yin, A., and Harrison, T.M., 2000, Geologic evolution of the Himalayan-Tibetan orogen: Annual Review of Earth and Planetary Sciences, v. 28, p. 211–280, https://doi.org/10.1146/annurev.earth.28.1.211.
Yu, M., Dilek, Y., Yumul, G.P., Yan, Y., Dimalanta, C.B., and Huang, C.-Y., 2020, Slab-controlled elemental–isotopic enrichments during subduction initiation magmatism and variations in forearc chemostratigraphy: Earth and Planetary Science Letters, v. 538, p. 116217, https://doi.org/10.1016/j.epsl.2020.116217.
Zhang, C., Liu, C.-Z., Wu, F.-Y., Zhang, L.-L., and Ji, W.-Q., 2016a, Geochemistry and geochronology of mafic rocks from the Luobusa ophiolite, south Tibet: Lithos, v. 245, p. 93–108, https://doi.org/10.1016/j.lithos.2015.06.031.
Zhang, C., Liu, C.-Z., Wu, F.-Y., Ji, W.-B., Liu, T., and Xu, Y., 2017, Ultra-refractory mantle domains in the Luqu ophiolite (Tibet): Petrology and tectonic setting: Lithos, v. 286–287, supplement C, p. 252–263, https://doi.org/10.1016/j.lithos.2017.05.021.
Zhang, C., Liu, C.-Z., Xu, Y., Ji, W.-B., Wang, J.-M., Wu, F.-Y., Liu, T., Zhang, Z.-Y., and Zhang, W.-Q., 2019, Subduction re-initiation at dying ridge of Neo-Tethys: Insights from mafic and metamafic rocks in Lhaze ophiolitic mélange, Yarlung-Tsangbo suture zone: Earth and Planetary Science Letters, v. 523, p. 115707, https://doi.org/10.1016/j.epsl.2019.07.009.
Zhang, H., Harris, N., Liang, G., and Xu, W., 2010, The significance of Cenozoic magmatism from the western margin of the eastern syntaxis, southeast Tibet: Contributions to Mineralogy and Petrology, v. 160, no. 1, p. 83–98, https://doi.org/10.1007/s00410-009-0467-5.
Zhang, L.-L., Liu, C.-Z., Wu, F.-Y., Ji, W.-Q., and Wang, J.-G., 2014, Zedong terrane revisited: An intra-oceanic arc within Neo-Tethys or a part of the Asian active continental margin?: Journal of Asian Earth Sciences, v. 80, no. 0, p. 34–55, https://doi.org/10.1016/j.jseaes.2013.10.029.
Zhang, L.-L., Liu, C.-Z., Wu, F.-Y., Zhang, C., Ji, W.-Q., and Wang, J.-G., 2016b, Sr-Nd-Hf isotopes of the intrusive rocks in the Cretaceous Xigaze ophiolite, southern Tibet: Constraints on its formation setting: Lithos, v. 258–259, p. 133–148, https://doi.org/10.1016/j.lithos.2016.04.026.
Zhong, Y., Liu, W.-L., Tang, G.-J., Liu, N.-N., Liu, H.-F., Zeng, Q.-G., and Xia, B., 2019, Origin of Mesozoic ophiolitic mélanges in the western Yarlung Zangbo suture zone, SW Tibet: Gondwana Research, v. 76, p. 204–223, https://doi.org/10.1016/j.gr.2019.06.008.

Zhou, Q., Liu, Z., Lai, Y., Wang, G.-C., Liao, Z., Li, Y.-X., Wu, J.-Y., Wang, S., and Qing, C.-S., 2017, Petrogenesis of mafic and felsic rocks from the Comei large igneous province, south Tibet: Implications for the initial activity of the Kerguelen plume: Geological Society of America Bulletin, v. 130, no. 5–6, p. 811–824, https://doi.org/10.1130/B31653.1.

Zhu, D.-C., Chung, S.-L., Mo, X.-X., Zhao, Z.-D., Niu, Y., Song, B., and Yang, Y.-H., 2009, The 132 Ma Comei-Bunbury large igneous province: Remnants identified in present-day southeastern Tibet and southwestern Australia: Geology, v. 37, no. 7, p. 583–586, https://doi.org/10.1130/G30001A.1.

Zhu, D.-C., Zhao, Z.-D., Niu, Y., Mo, X.-X., Chung, S.-L., Hou, Z.-Q., Wang, L.-Q., and Wu, F.-Y., 2011, The Lhasa terrane: Record of a microcontinent and its histories of drift and growth: Earth and Planetary Science Letters, v. 301, no. 1–2, p. 241–255, https://doi.org/10.1016/j.epsl.2010.11.005.

Zhu, D.-C., Zhao, Z.-D., Niu, Y., Dilek, Y., Hou, Z.-Q., and Mo, X.-X., 2013, The origin and pre-Cenozoic evolution of the Tibetan Plateau: Gondwana Research, v. 23, no. 4, p. 1429–1454, https://doi.org/10.1016/j.gr.2012.02.002.

Ziabrev, S., Aitchison, J., Abrajevitch, A., Badengzhu, Davis, A., and Luo, H., 2003, Precise radiolarian age constraints on the timing of ophiolite generation and sedimentation in the Dazhuqu terrane, Yarlung-Tsangpo suture zone, Tibet: Journal of the Geological Society [London], v. 160, no. 4, p. 591–599, https://doi.org/10.1144/0016-764902-107.

Science Editor: Rob Strachan
Associate Editor: Timothy Kusky

Manuscript Received 29 January 2020
Revised Manuscript Received 4 June 2020
Manuscript Accepted 14 July 2020

Printed in the USA